Chapter 4.

Mineral Geodynamics.

October_9_2016.

4.1. Introduction.

In Chapter 1 we described hydrothermal systems as resulting from an energy cascade process whereby energy is supplied to the system at a coarse scale arising from relative movements of parts of the lithosphere of the Earth. This energy is cascaded down the spatial scales by processes that dissipate energy at these various scales. As such, geotectonic processes are fundamental to understanding hydrothermal systems. These coarse scale processes are also responsible for supplying and localising heat and fluids that drive the evolution of hydrothermal systems. Thus hydrothermal systems are closely linked to processes resulting from plate tectonics and global dynamics. A robust understanding of the generic controls on hydrothermal systems formation is the first step in solving the mineral system puzzle. Hydrothermal systems form in a number of geotectonic settings. Here we will divide these settings into two categories – horizontal tectonics and vertical tectonics (Figure 4.1). Under the umbrella of horizontal tectonics, plate tectonic features are taken into account: ocean ridges, subduction/accretion. Vertical tectonics includes all types of instabilities within the lithosphere such as classical Rayleigh-Taylor instabilities and plastic instabilities or *delamination* by "peeling off" slabs of lithosphere.

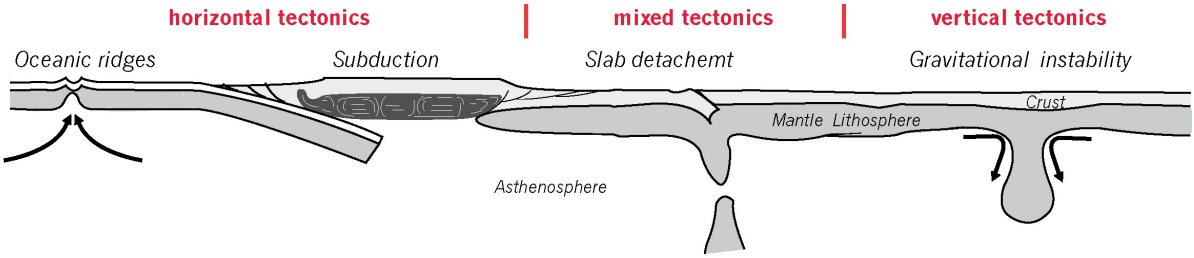

Figure 4. 1. Schematic scenarios for tectonic processes controlling hydrothermal systems involving interaction of the asthenosphere, mantle lithosphere and crust. These scenarios include: horizontal tectonics: oceanic ridges and subduction, vertical tectonics: gravitational instabilities, and mixed tectonics: slab detachment.

The length scales associated with mineralised systems (100's of kilometres) imply that interaction between mantle lithosphere-crust and asthenosphere is a critical element in understanding hydrothermal systems. Therefore in the first part of this chapter (section 4.1) we will discuss the term *lithosphere*. Following we will discuss how instabilities in the lithosphere can be formed and (Section 4.2) how they can control magmatic and tectonic systems in the continental crust. These processes need deep understanding as vertical tectonics was most likely the dominant tectonic process during Archean (time of formation for over 60% of gold deposits) and therefore is the gateway into understanding the formation of a large number of deposits. We then consider some aspects of subduction processes, in particular slab melting (Sections 4.3 and 4.4) and slab devolatilisation concentrating mainly on CO_2 generation, propagation, metasomatism and reactivation. In Section 4.5 we examine the generation of CO_2 during crustal metamorphism. Finally (Section 4.6) we examine

tectonic processes that may have characterised environments that dominated the Earth prior to about 3 Ga when plate tectonics began. We conclude with a summary in Section 4.7.

The title of this chapter, *Mineral Geodynamics,* is chosen to emphasise that we are interested in more than those processes that lead to subduction and delamination; we also want to understand the processes, at the global scale, that produce heat and fluids to drive the evolution of hydrothermal systems. In particular we want to understand how short lived (<<10 my) pulses of CO_2 and H_2O, localised at length scales of ~100 km and associated with localised periods of extension and alkaline igneous rocks, can develop. These are the regional characteristics of interest in exploration for orogenic gold deposits.

The discussion below concentrates on the assumptions built into the computer code, I2ELVIS, that is used in the simulations presented in this chapter.

4.1.1. The lithosphere of the Earth.

The lithosphere (Ancient Greek: λίθος [lithos] for "rocky", and σφαῖρα [sphaira] for "sphere") is the strong outermost shell of a rocky planet. The concept of the lithosphere as Earth's strong outer layer was developed by Joseph Barrell; who wrote a series of papers introducing the lithosphere. The concept was based on the presence of significant gravity anomalies over continental crust, from which he inferred that there must exist a strong upper layer (which he called the lithosphere) above a weaker layer, which could flow (which he called the asthenosphere). These ideas were expanded by Daly (1940), and have been broadly accepted by geologists and geophysicists. Although these ideas about lithosphere and asthenosphere were developed long before plate tectonic theory was articulated in the 1960s, the concepts that a strong lithosphere exists and that this rests on a weak asthenosphere are essential to that theory.

There are several definitions of the lithosphere:

(1) The mechanical (kinematic) lithosphere is the uppermost layer of the solid Earth characterized by relatively slow visco-elastic relaxation, in contrast to the underlying, relatively low viscosity asthenosphere. The implication is that the layer is strong enough to resist small-scale convection – based on the concept that there is a relatively thin layer of convection cells at the base of the mantle. It has been shown that when oceanic lithosphere reaches a critical thickness, small-scale convection develops, accompanied by convective erosion occurring at the base of the lithosphere. The long-term mechanical base of the kinematic lithosphere is limited by the depth to the 500-600°C isotherm in oceans and the 700-800°C isotherm in continents.

(2) The thermal lithosphere is that part of the Earth where the dominant mode of heat transfer is conduction. The thickness must be extrapolated from surface heat flow data or from lithospheric base pressure and temperature estimates based on xenolith data. The base of the thermal lithosphere is set at 1330°C.

(3) The elastic lithosphere is that part of the outer Earth that can be considered to act as an elastic plate under short term deformations. The thickness, T_e, is that of an equivalent elastic layer; it can be estimated by observations on glacial unloading but does not correspond directly to any specific structure in the lithosphere.

(4) The seismic lithosphere is determined from seismic observations; its base corresponds to the top of the low velocity zone (LVZ), presumably where the mantle is close to the solidus temperature (the appearance of significant amounts of partial melting), or, alternatively, as a natural consequence of a thermal boundary layer and the effects of pressure and temperature on the elastic wave velocity of mantle components in the solid state.

(5) The petrologic lithosphere is that upper layer of the Earth that maintains a distinct chemical/isotopic character over time. As the lithosphere is heated it may become more like the asthenosphere in its physical properties, but maintains its "lithosphere" chemical and isotopic characteristics. The petrological lithosphere has a slightly lower density than the underlying asthenosphere and so is relatively buoyant. The lower density supposedly originates from the extraction of basalts over time.

(6) The plate tectonic lithosphere is a relatively strong upper layer of the Earth that moves as a unit in plate tectonics.

This multiple usage of the term lithosphere is an indication (perhaps surprisingly) that no thermodynamically unified mechanical-thermal-chemical theory of plate tectonics yet exists. Such a theory presumably follows the lines of that developed for some atmospheric weather systems. The proposal for these systems is that cooling of the atmosphere can take place by two modes. One is (slow) radiative heat transfer into space and the second is by (fast) convective motions which constitute storm systems. Competition between these two processes leads to the atmosphere dividing into broad regions where the radiative mode dominates and localized fronts or low pressure regions where the convective mode dominates. The process is called *self-aggregation*. Presumably a similar process operates in the outer part of the Earth: broad regions (the plates) form where the dominant mode of cooling is by conduction and these are separated by narrow regions (the plate margins) where (fast) convective heat transfer dominates. The broad regions are mechanically close to instability and can fail internally by convective motions recognized as Rayleigh-Taylor instabilities or delamination.

The most useful definition of the lithosphere may be in the sense that the term was originally employed, in terms of its mechanical properties. "Lithosphere" is a mechanically strong portion of the crust and/or mantle that does not undergo significant viscous relaxation on the time scale of interest and deforms elastically up to the point that it fails in a brittle fashion. A yield strength envelope (Figure 4.2) shows the relative importance of temperature and pressure changes in the brittle and ductile regimes of rock deformation. The result is asymmetric and emphasises that the strength of the brittle-ductile transition is significantly larger and shallower in compression than in extension. The area under the yield strength envelope leads to the integrated strength, which is a measure of the total lithospheric strength. This implies that (1) the integrated yield strength transmits the global plate tectonic stress field and (2) the driving forces of plate tectonics cannot exceed the integrated lithospheric strength. This provides an important constraint on the geodynamics of oceans and continents.

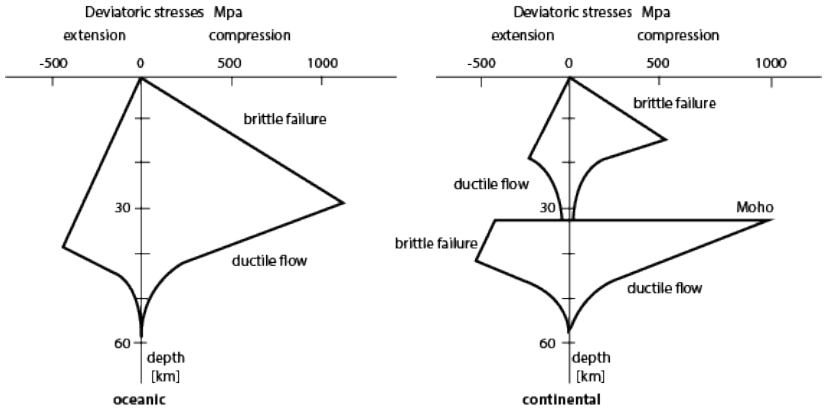

Figure 4.2. Typical yield stress envelopes for lithospheric flexure. The depth to the ductile flow regime depends on composition, the geothermal gradient and strain rate. Compositional stratification in the continents sometimes leads to the development of a crustal asthenosphere separating upper crustal and uppermost mantle lithospheres.

Strength profiles of oceanic lithosphere have simple shapes. The basaltic crust has a near zero thickness at the mid oceanic ridge and the thin sedimentary cover is too small to influence the overall rheology of the whole lithosphere. The oceanic crust thickens to about 5-7 km by cooling of the sub-crustal mantle lithosphere. Thus, the bulk composition of an oceanic lithosphere is rather uniform and the rheology of olivine is assumed to govern its bulk behaviour. Strength profiles first increase linearly with depth according to the Byerlee law (see Box), then decrease exponentially according to the olivine viscous power law to grade into the weak asthenosphere (etymology: strength-less sphere). Since Byerlee's law applies independently of the rock-type, the presence of plagioclase and pyroxene in the cold crust of basalts and gabbros is neglected. The brittle and viscous yield envelopes intersect at the brittle-ductile transition.

The strength-profile concept is more complex to apply to continents where the crust is compositionally heterogeneous (Figure 4.3) and thicker than in oceans. The rheology of the crust is generally approximated as that of the most common mineral, wet quartz, which is brittle at shallow depth but typically ductile at temperatures >300-350°C, well above the Moho (about 500°C). If the crust deforms at constant strain rate, then its brittle strength increases with depth and crosses the viscous strength envelopes at the "brittle-ductile" transition, at about 15 km depth for a typical geothermal gradient of 20 °C km^{-1}. The crust above this depth deforms in a brittle fashion.

Below this depth the crust is viscous and the viscous strength decreases with depth. The brittle ductile transition supports the highest shear stresses anywhere in the crust and it is within this depth range that the highest moment release might be anticipated from intraplate earthquakes. At increased strain rate, the viscous stresses become larger so that the brittle ductile transition moves downwards and *vice versa*. Below the Moho, the viscous curve for wet quartz is replaced by that for olivine. Olivine supports substantially higher shear stresses than quartz and the Moho is therefore the region of highest strength in the lithosphere. As for

the oceanic lithosphere, the thickness of the continental mantle lithosphere is age-dependent, being the thickest under oldest cratons.

Known experimental data seem to indicate that the lower crust is markedly weaker than the peridotite mantle immediately above the Moho. As a consequence, the continental lithosphere has one (at the bottom of the crust) or two (the previous one plus another at mid-crustal levels) soft ductile layers sandwiched between brittle layers. The rheological layering may be complicated if the lower crust is mafic or granulitic. In that case the rheology of plagioclase or dry quartz, respectively, is applied. Molten rocks may be significantly weaker, resulting in decoupling horizons where contrasting rheologies occur. In that perspective, the continental mantle can be attenuated by positive thermal anomalies due to, for instance, delaminated cold lithosphere. In that manner, one may include many layers and quite a variety of strength profiles for the continental lithosphere. Yet, the integrated strength for the continent will usually be less than that of the ocean of same age.

BOX: **Byerlee law in a nutshell:**

Byerlee's friction law (empirically derived from experimental determination of "maximum shear stress" on a wide range of rock types) is based on the concept of Coulomb's friction law for pre-existing fault surfaces and predicts a linear increase of rock strength with depth following the following relationship: $\tau = c + \mu\sigma_N$, where τ is the shear stress at failure of a pre-existing fracture, σ_N is the effective normal stress, c is known as the cohesion and μ is the coefficient of friction. Byerlee determined μ to be 0.85 and c = 0 at confining pressures up to 200 MPa, and μ= 0.6 and c = 800 bars at greater confining pressures. The strength increase with depth differs between extensional, strike-slip, and compressional situations due to the different orientation of fractures and normal stresses on them (Anderson's fault model). Apparently the frictional strength is rather independent of mineralogy, strain rate, and temperature, however, each of these parameters may have some effect. Other interpretations of the strength of the crust are illustrated in Figure 4.3.

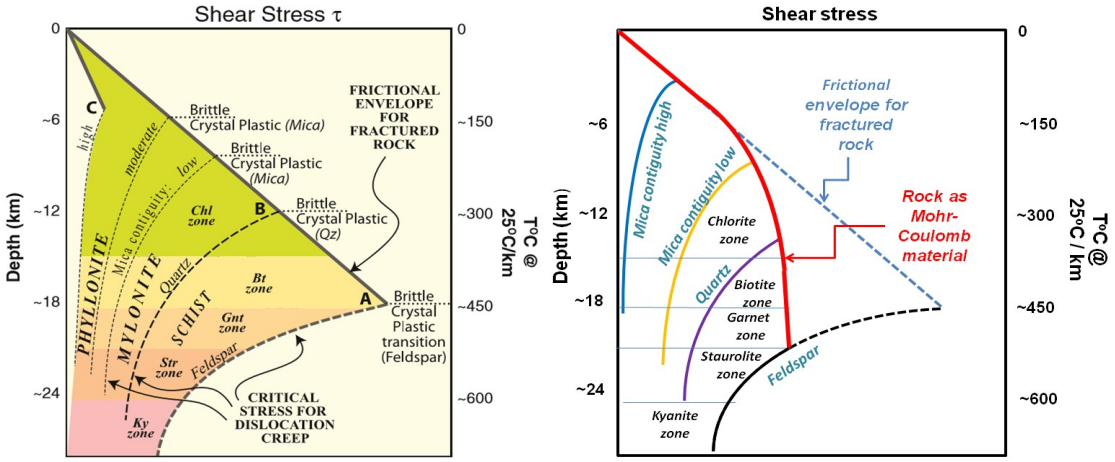

Figure 4.3. Examples of the relation between the strength envelope defined by Byerlee's law and other possible relations for strength in the crust. Byerlee's law defines an upper limit for the stress that the crust can support. The left hand side shows posssibilities for strength of the crust if it is dominated by mica (without and with

strong contiguity), quartz or feldspar. The right hand side shows further modification if the constitutive behaviour is considered Mohr-Coulomb as opposed to frictional Coulomb-Navier.

4.2. Lithospheric gravitational instabilities.

Gravitational instabilities form mainly in regions with higher density than the material horizontally adjacent to them. Many researchers have focused on instabilities formed through crustal thickening, for example, during a convergent orogeny, others have suggested that phase changes in the deepest regions of lithospheric roots may add to density instabilities. If a lithospheric root is pushed into the eclogite stability field it may then become denser than its surroundings due to phase changes. As a consequence removal of the lower lithosphere (mantle lithosphere with or without portions of the crust) through ductile gravitational instabilities can produce magma under continents. Hence, we will expand on the need for density variations for lithosphere to be unstable. However at first let us look at the conditions under which the lithosphere is stable.

4.2.2. Stability of the lithosphere.

In a steady state, the transition from the lithosphere to asthenosphere is on the verge of stability. This determines its depth, thickness, and the steady-state temperature distribution. Had the mantle been homogeneous (which of course it is NOT), the base of the lithosphere at the current potential temperature would lie globally at the same depth, H_{rh} , of 50 to 70 km (Figure 4.4). Actually, the regime of interaction of the mantle with the lithosphere is determined by the relationship between this depth and the thickness, H_{cbl}, of the chemical boundary layer (CBL) including the crust and the depleted mantle (Figure 4.4). If the thickness of the chemical boundary layer is small $H_{depl} < H_{rh}$, as it is in the case of the present-day oceanic mantle, the oceanic regime is established with mantle convection that does not reach the base of the chemical boundary layer (Figure 4.4). In this case, the top of CBL is located at depth H_{rh} , while the oceanic heat flow and the depth of the seafloor only depend on the potential temperature, T_p , and, within the areas where the crust is older than 60 to 70 Ma, is the same everywhere far from the disturbed territories (hot points and the subduction zones). The absence of noticeable distinctions between the heat-flow in the different oceanic basins suggests a global constancy of the potential temperature.

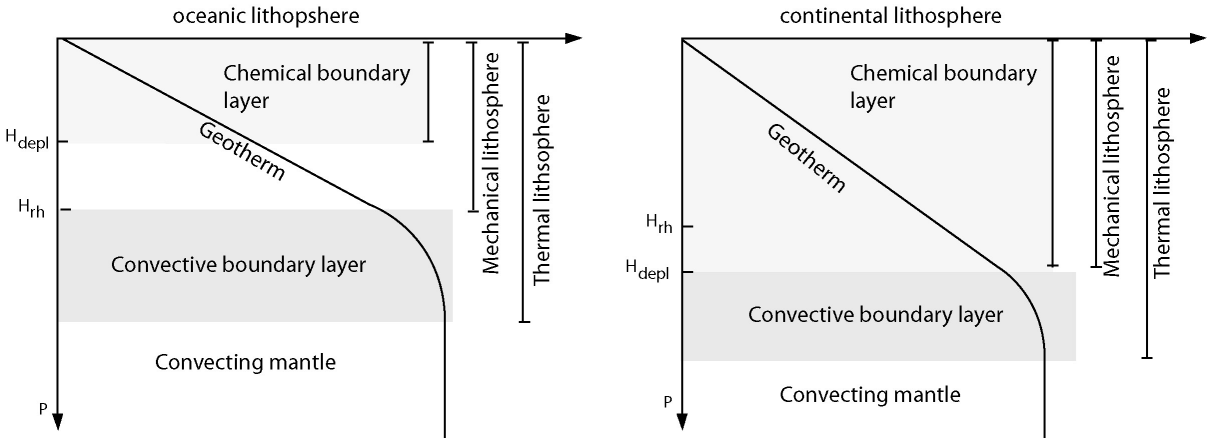

Figure 4. 4. The thermal structure of the model: (left) the oceanic regime of interaction of the mantle convection with the lithosphere ($H_{depl} < H_{rh}$) ; (b) the continental regime ($H_{depl} > H_{rh}$).

In the case of continental lithosphere if $H_{depl} > H_{rh}$ (frequently the case), the interaction of mantle convection with the chemical boundary layer is well established. In this case, the CBL is immediately adjacent to the depleted lithosphere, its top is located at depth, H_{depl} , and the surface heat flow $q(T_p, H_{depl})$ not only depends on the potential temperature T_p but also on the thickness of the mantle lithosphere H_{depl} ; it decreases with increasing H_{depl} and, therefore, with the age of the lithosphere. As an example, the thickness of the mantle lithosphere appreciably influences both the surface and the sub-lithospheric heat flow. Thus at T_p = 1350°C, the decrease in H_{depl} from 200 to 75 km is accompanied by an increase in the heat flow from 38 to 58 mW m^{-2} (radiogenic heat production not taken into account) and an increase in the sub-lithospheric heat flow from 16 to 33 mW m^{-2}.The outcome is that the continental lithosphere is unstable when young and shallow is vulnerable to heating/melting.

4.2.2. Mechanical removal of the mantle lithosphere

Continental lithosphere, in addition to being mechanically eroded by small-scale convection at its base, is exposed to another group of mechanisms based on dynamic interaction between the lithosphere and underlying mantle. There are two primary removal mechanisms proposed: (1) lithospheric ‘‘dripping,’’ initiated by a viscous *Rayleigh-Taylor instability* of the mantle lithosphere and (2) *delamination* (Figure 2.16), a wholesale peeling away of a coherent block of the mantle lithosphere.

Rayleigh-Taylor Instabilities. The classical concept of a Rayleigh-Taylor instability involves the behaviour of an interface between two inviscid, incompressible materials of different densities, ρ_1 and ρ_2 with $\rho_2 > \rho_1$ (Figure 4.5). One of the simplest and insightful analyses of the instability is given by Pritz (2009): If we consider a perturbation of amplitude $\xi(x)$ as shown in Figure 4.5 then a pressure difference, $\Delta p = (\rho_2 - \rho_1)g\xi$, exists across the interface and tends to deform the interface further. Newton’s second law of motion then gives $m\ddot{\xi} = A\Delta p$ where A is the area of the interface, m = m_1 + m_2 is the mass of both fluids involved in the motion and the double over dots represent double differentiation with respect to time, t. It is assumed that any instability is a surface mode that decays away from the interface as exp(-ky) where $k = \frac{2\pi}{\lambda}$ is the wave-number of the instability with wavelength, λ. Then $m = \rho_1 \frac{A}{k} + \rho_2 \frac{A}{k}$ and we obtain:

$$\frac{\rho_2 + \rho_1}{k}\ddot{\xi} = (\rho_2 - \rho_1)g\xi \qquad (4.1)$$

or (4.2)

with $A_T = \frac{\rho_2 - \rho_1}{\rho_2 + \rho_1}$

(4.2) can be integrated to give an asymptotic exponential amplitude growth rate, $\gamma = \sqrt{A_T kg}$. A_T is known as the Atwood Number. One of the issues with instabilities driven

by density differences, as indicated by this expression for γ, is that the growth rate for short wavelengths is unbounded so that the problem as it is conventionally framed is ill-posed mathematically. It is found that this derivation is true only for small ξ, with a limit of perhaps $\xi = 0.1\lambda$. For larger ξ, nonlinear terms become important and there are no analytical solutions available. For the lithosphere/asthenosphere contact, $\rho^{asthenosphere} = 1.015\rho^{lithosphere}$ so that according to the classical view of the Rayleigh-Taylor instability, driven solely by density contrasts, the lithosphere/asthenosphere interface is stable.

One can generalise the discussion to materials with more complicated rheological properties other than inviscid and incompressible material behaviour by thinking of the surface instabilities of the type discussed above as *acceleration instabilities,* where instabilities arise because of processes induced by forces normal to the interface. Thus if there are *i* different forces, F_i, acting across the interface then Newton's second law of motion becomes:

$$\frac{d}{dt}[(m_1 + m_2)\dot{\xi}] = (\rho_2 - \rho_2)kg\xi + \sum_i F_i \qquad (4.3)$$

and this is the equation that now describes the initial evolution of the surface instability. Notice that, in principle, the instability can form when $\rho_1 = \rho_2$ when there is no density contrast across the interface or even if $\rho_2 > \rho_1$, as is proposed for the lithosphere/asthenosphere interface, so long as $(\rho_2 - \rho_2)kg\xi < \sum_i F_i$.

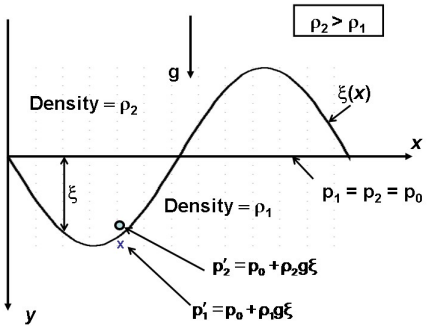

Figure 4.5. An interface between two materials with densities ρ_2 ,above, and ρ_1 ,below, with $\rho_2 > \rho_1$. The interface is perturbed by $y = \xi(x)$ and subjected to an acceleration due to gravity, g. The pressure difference across the interface for a perturbation, ξ , is $\Delta p = (\rho_2 - \rho_1)g\xi$.

Other physical parameters that result in a force normal to the interface and that have been explored include heterogeneity, anisotropy, surface tension, elasticity, viscosity and plasticity. In particular the introduction of elasticity and viscosity tends to regularise the problem so that the growth rate of small and large perturbations is reduced and in the linear approximation a single dominant wavelength is preferred. Heterogeneity and anisotropy

introduce nonlinearities that excite localised (and hence, non-sinusoidal and asymmetrical) responses.

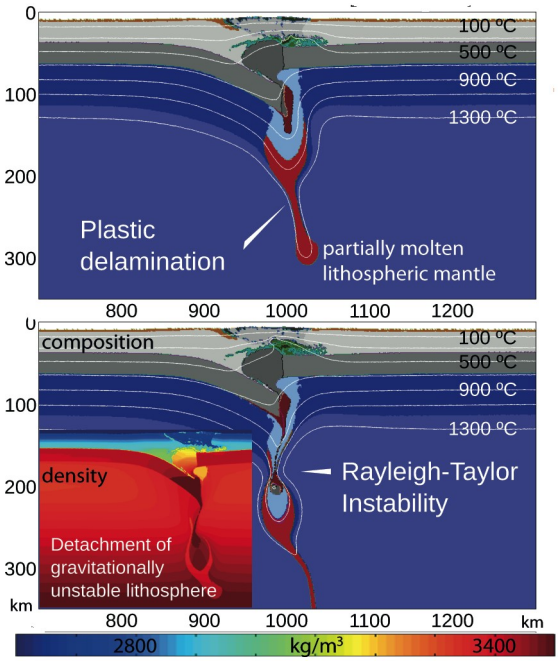

Figure 4.6. Example of two acceleration instabilities developed in thickened continental lithosphere. The thickening arises from compression of heterogenous continental lithosphere (weak zone generated by lowered yield point due to introduction of H_2O). At first the development of plastic delamination at the interface between asthenosphere and partially molten mantle lithosphere is triggered by surface tension between the media. This is followed by gravitational instability triggered by the density contrast between the media. Color code as in Figure 2.16. Results from numerical modeling performed using the computer code, I2ELVIS.

Although the terms Rayleigh-Taylor and gravitational instability should strictly be reserved for instabilities generated solely by a density difference across an interface normal to the gravity field, we (in common with much of the recent literature) use these terms to refer to any instability generated at an interface arising from forces normal to that interface. As indicated above, a general term for this class of instabilities is an *acceleration instability.*

Although the acceleration instability concept has been discussed many times in the literature we emphasise here that the plastic properties of the lithosphere are important and perhaps dominant in controlling the development of the instability rather than previously emphasised viscous properties or density contrasts as in the strict Rayleigh-Taylor instability.

Small-scale thermal convection can develop within a convective boundary layer (as mentioned above) and also when lowering of the yield point occurs (Figure 4.7) in the mantle lithosphere due, for instance, to the introduction of fluids or a preceding tectonic/magmatic event. This triggers the minimal bulging at the lithosphere/asthenosphere interface necessary to initiate acceleration instabilities.

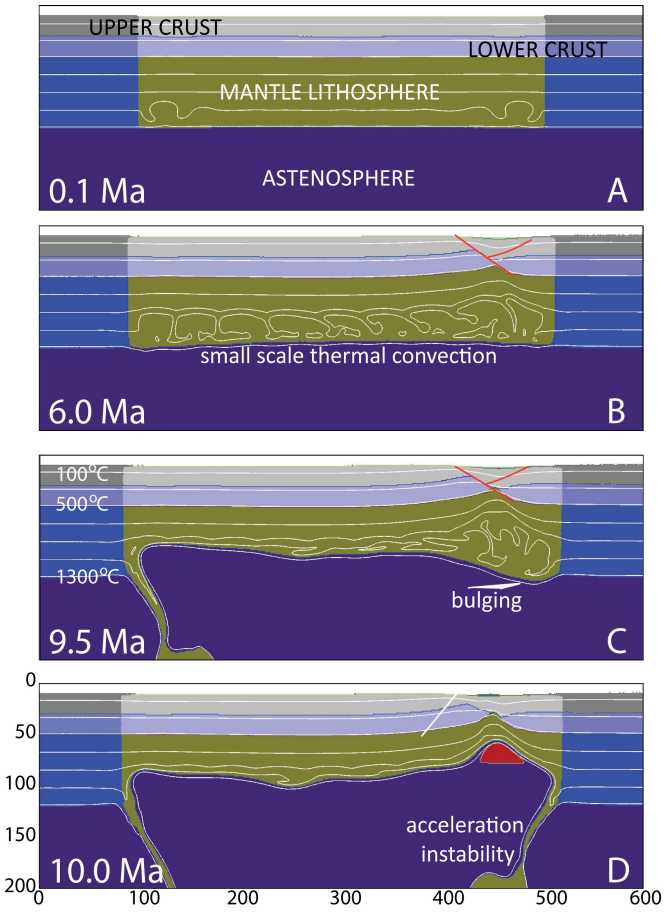

Figure 4.7. Example of acceleration instability triggered by small scale convection developed at the base of mantle lithosphere within a zone with lowered yield point after minimal extension triggered by external forces. Color code as in Figure 2.16. Results from numerical modelling performed using I2ELVIS.

Delamination. Bird proposed a model of mantle lithosphere delamination, where the cold and dense mantle lithosphere peels away as a coherent slice from the crust along the Moho; an example is where a brittle oceanic plate falls away from beneath a collisional orogen. This process was christened ‘‘flake tectonics’’. The removed slice of mantle lithosphere is replaced by underlying hot and buoyant asthenosphere (Figure 4.8). Generally, this form of delamination is predicated on the idea that the hot-weak lower crust is the most pronounced strength discontinuity in the lithosphere. This results in separation (or delamination) between the strong crust and strong mantle lithosphere portions of the plate.

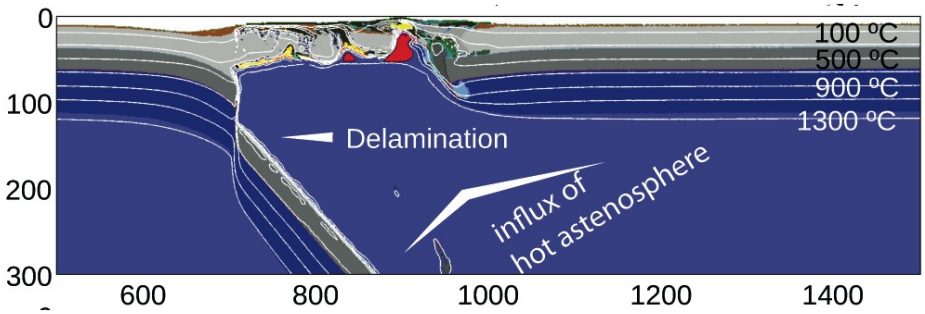

Figure 4.8. Example of mantle lithosphere delamination and the introduction of mantle lithosphere. Color code as in Figure 2.16. Results from numerical nodeling performed using I2ELVIS.

The acceleration instability and subsequent delamination of part of the lithosphere is a viable mechanism for intra-plate tectonism and may be quite common. Some examples are the Carpathian–Pannonian system of Eastern and Central Europe, the Proterozoic Nampula Complex, northern Mozambique, lithospheric delamination beneath the Alboran Sea and Rif-Betic mountains, lithospheric delamination in the core of Pangea, the "Great Basin Drip" in Nevada and lithospheric deformation in the South Island of New Zealand, and the Musgrave orogeny in Central Australia.

4.3. Meting and instabilities in the mantle lithosphere.

Since the 1960s, many studies have invoked strong thermal anomalies associated with the existence of mantle plumes, whose origins have been placed near the mantle–core boundary, or upper–lower mantle transition zone as the main cause of both oceanic and continental (apart from continental collision zones) intra-plate magmatism. In many continental flood basalt provinces (mostly at the boundaries of two cratonic blocks), the active role of mantle plumes has been invoked to explain the high melt productivity. In this chapter we explore deformation and melting of plates interiors caused by other vertical processes, where the existence of mantle plumes is not required, and the melting is efficient and versatile. We will concentrate on three types of melting: (i) melting triggered by a gravitational instability, (ii) melting of the down going "drip", and (iii) melting triggered by "peeling off" or delamination.

BOX: MELTING OF THE MANTLE

There are three fundamental ways to cause the mantle to melt and produce magma:

(i) Bring the material closer to the surface resulting in melting through depressurization;
(ii) Change the composition of the material such that its melting point is lowered; and
(iii) Increase the temperature of the material.

Process one, melting through adiabatic decompression, is the main process that operates at mid-ocean ridges. Beneath ridges, there are upwelling zones in which melting begins at about 50 km depth.

Process two, changing the composition of the material, is the main process that operates in subduction zones. Material in the mantle wedge is brought to higher pressures as it goes through the corner flow and begins to descend with the slab, so there is only a small region in which decompression can occur, before the corner of the wedge is reached. In subduction zones, melt is predominantly created by the addition of incompatible chemical species that rise off the slab, mainly water, sodium, and potassium. The addition of these elements, which are not accommodated within common mantle mineral crystal structures, acts thermodynamically to reduce the temperature of melting of the mantle, sometimes by as much as 200°C or more. In this situation, mantle material can melt without changing its pressure or temperature.

Process three, increasing the temperature of a piece of mantle material, is a slow, low-volume process that can only operate in specialized circumstances where very hot material is brought into contact with colder material, and the colder material heats up conductively. This is an inefficient process that appears to have little bearing on the production of major volumes of primary volcanic magma on Earth.

4.3.1. Melting triggered by gravitational instability.

After the development of a gravitational instability by, for example, mechanical thickening of the lithosphere, eclogitisation (density increase), or combinations of both, the unstable part of the lithosphere forms a “blob” (Figure 4.9 a), which subsequently detaches from the surrounding lithosphere and sinks into the hot asthenosphere (Figure 4.9 b). After detachment, thermal equilibration takes place, which leads to rapid temperature increase at the base of the crust above the delaminated material (Figure 4.9 c). Such thermal anomalies lead to partial melting of the lower continental crust at temperatures exceeding the Moho temperature by 200 - 300ºC. This is the main melting event. Batholiths can be formed, sourced from the lower crust (their size depends on the drip size), at mid to upper crustal levels and may reach the surface in subsequent tectonic events, such as crustal rebounds.

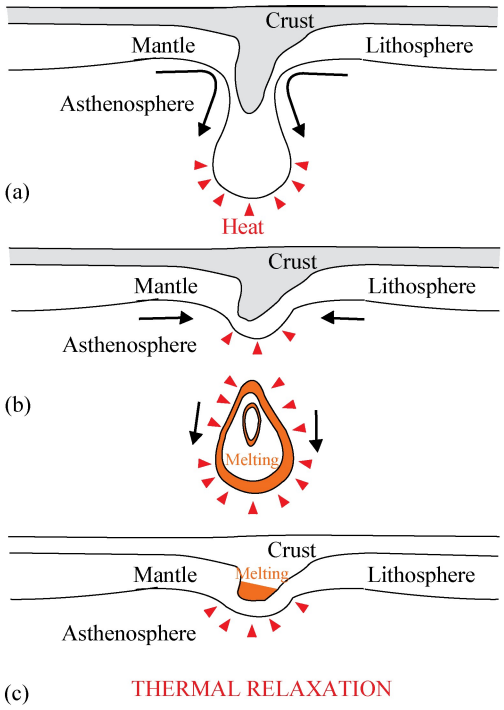

Figure 4.9. Sketch representing detachment of gravitational instablilty and thermal/melting response to this process

An example of a numerical experiment representing a gravitational instability (using the I2VIS code) is presented in Figure 4.10. In the left-hand side panel one can see extensive melting (brown) of the lower crust after detachment of the down-welling lithosphere, followed by thermal rebound and rapid increase of temperature in the crust (see isotherms in Figure 4.10), this results in increased melting of the lower crust (Figure 4.10). It needs to be stressed that in the case of a gravitational instability of relatively symmetrical geometry the melt temperatures are moderated and the main source of melt is in the lower crust.

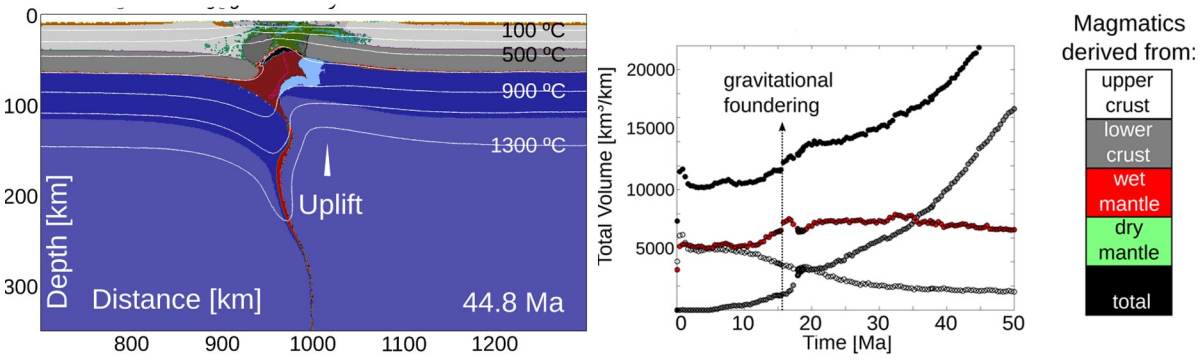

Figure 4.10. Example of of melting patterns and behaviours as a result of asymmetric mantle delamintion Color code as in Figure 2.16. Results from numerical nodeling performed using I2ELVIS.

This type of behavior is quite common in nature. Here, as examples, we will concentrate on adakites and anorthosites. Adakites are considered by many to be associated with subduction zones. However, the origins of some adakitic rocks have also been attributed to several alternative mechanisms, such as partial melting of thickened lower crust or

delaminated mafic lower crust, and to assimilation and fractional crystallization (AFC) processes acting on mantle-derived mafic magmas. As an example we address here felsic adakites in the Yangtze Block and the Dabie Orogen, in eastern China. Field relations, isotope systematics, and plate tectonic reconstructions clearly indicate that they were not derived from a subducting slab. These adakites are thought to originate from deep melting of the lower crust, and can occur after delamination of a gravitational instability, resulting from the thermal equilibration of the system and fast temperature increases at the base of the Moho.

Several anorthosite provinces found in Canada coincide with structural weakness in the lithosphere, which appears to control and favour the emplacement of diapirs. Indeed, the Nain anorthosite province straddles the limit between the Nain and Churchill (Rae) Provinces; the Lac St Jean and Havre-St. Pierre anorthosite complexes are associated with long lineaments; in the Laramie anorthosite complex, two generations of anorthosites are linked to a terrane boundary. The Suwalki anorthosite was emplaced in the Svecofennian platform along an E-W lineament.

The origin of voluminous anorthosite, mangerite, charnockite, granite, and related granitoids in the Mesoproterozoic Grenville province is a matter of considerable debate. The association of crustal thickening, emplacement of mafic dikes and voluminous mantle-derived melts, sedimentation within an intraplate setting, and syn-collisional extension can be best explained by replacement of the continental mantle lithosphere by asthenosphere during crustal shortening. Replacement of lithosphere by asthenosphere is predicted by convective thinning models, providing a viable mechanism for such a process during convergent tectonism, and does not necessitate the postulation of a mantle plume beneath a supercontinent (Hoffman, 1989) nor post-collisional extension. With respect to the Grenvillian orogeny, the convective thinning model provides a plausible way to explain the episodic nature of AMCG-type magmatism synchronous with contractional tectonics. Additionally, it provides a mechanism to explain the contribution of mantle-derived heat that is necessary for the formation of anorthosite, which is also implied from the generally high ambient grade of metamorphism accompanying AMCG-type magmatism.

4.3.2. Melting of the drip.

As the drip submerges into hot asthenosphere, it is surrounded from all sides by material hotter by >200°C. Such an environment leads to immediate heating and melting of the "blob material" (Figure 4.9 b). The molten material can make its way to the crust and surface. One point that needs to be taken into account is the fact that the "blob" sinks at relatively fast rates of 20 – 30 cm/yr. Therefore most melt release can take place when the "blob" is still attached to the lithosphere or when it stagnates at the 410 or 660 discontinuity in the asthenosphere.

4.3.3. Melting triggered by delamination.

Lithospheric delamination occurs when the detachment process develops asymmetrically and is followed by "peeling off" of mantle lithosphere. After the detachment,

when the system develops an asymmetric geometry, hot asthenospheric material can intrude into the lithosphere. As a consequence, decompression melting of the dry peridotitic mantle and horizontal melt intrusion at crustal levels occurs. Mantle lithosphere (mantle lithosphere with a portion of the crust) decouples, peels away, and finally detaches as the density of the subducting part increases during eclogitisation of the sinking material. The occurrence of extension in the remaining crust enables additional asthenospheric inflow of hot mantle material to shallow depths; this results in ultra-high temperatures at very shallow levels (over 900ºC at depths of 30km). Such elevated temperatures (exceeding 900ºC) promote melting of all types of rocks, even under dry conditions. Due to the localized input of hot material, rocks experience melting under different thermal and pressure conditions – from the centre of the heat influx to its flanks. This behaviour is confirmed by numerical modelling in Figure 4.11 where one can observe zonation of melt with hot mafic melts (exceeding 1000ºC, decompression melting) flanked by mixed suites with melts occurring at a range of temperatures (600 - 1000ºC). Metamorphosed zones where temperatures did not reach the melting point surround these suits. It is emphasised that in the case of an asymmetric gravitational instability the melt temperatures can be ultra-high and a range of melt compositions can develop.

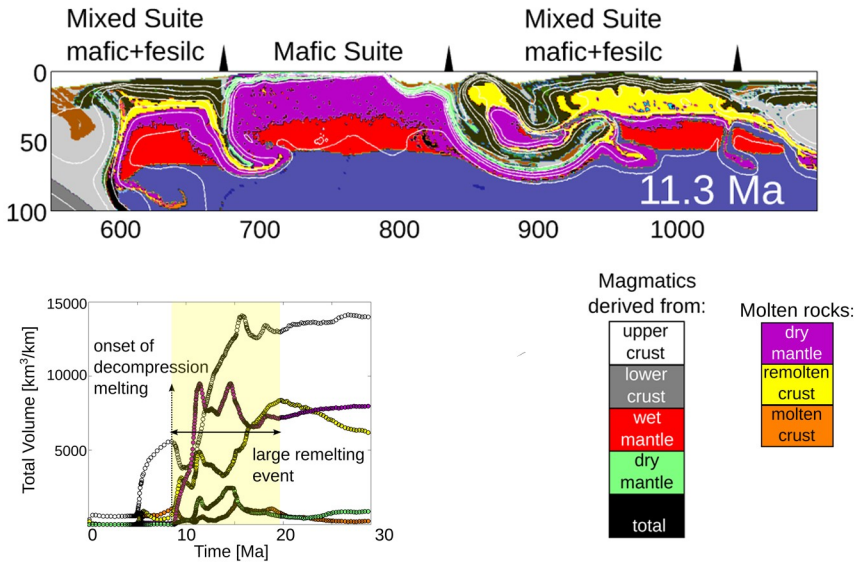

Figure 4.11. An example of melting patterns and behaviours as a result of asymmetric mantle delamintion. Color code as in Figure 2.16. Results from numerical modeling performed using I2ELVIS.

As an example of extensive melting resulting from "flake tectonics" we present a model of the Musgrave Province, which lies at the convergence of three major crustal blocks: the North, West and South Australian cratons. These cratons are interpreted to have amalgamated prior to c. 1290 Ma. The Musgrave Orogeny has been interpreted as an intra-continental orogeny and has been dominated by ultrahigh-temperature (UHT) conditions, which have persisted from c. 1220 Ma to c. 1120 Ma. Granites emplaced at temperatures ≥1000°C from c. 1220 Ma to c. 1150 Ma dominate the west Musgrave province. The onset of UHT metamorphism coincided with a change from low-Yb to voluminous high-Yb granite

magmatism, reflecting a change to melting at lower pressures linked to a rapid decrease in crustal thickness. UHT magmatism and UHT metamorphism are related to the same thermal anomaly but the metamorphism is not a direct result of granite magmatism. UHT metamorphic conditions of ≥1000°C at 7-800 MPa (i.e. ~ 25 km depth) reflect a very thin crust (including crustal lithosphere), with a maximum thickness of ~ 35 km throughout the duration of the Musgrave Orogeny. The geochemical and isotopic homogeneity of the granites over a scale of >15 000 km^2 reflects a similarly homogeneous source. This source included an old enriched felsic crustal component but also incorporated >50% of mantle material. Pulsed addition of mantle magma resulted in at least four distinct granite age peaks each with a corresponding metamorphic age peak that occurs ~ 10 Myr later. The duration of UHT metamorphic conditions that characterises the Musgrave Orogeny is inconsistent with a mantle plume and hence other geodynamical models involving delamination have been proposed. The Musgrave Province itself is rigidly fixed at the nexus of three thick cratonic masses (North, West and South Australia cratons). Therefore, this geotectonic position may have provided a focus for both asthenospheric upwelling and far-field stresses acting on relatively thin lithosphere, producing periodic (pulsed) tectonic instabilities under a regime of a more continuous supply of both heat and mantle-derived magma.

4.4. Melting and subduction.

Two volatile components stand out as the most geologically significant in the chemical evolution of the Earth: water (H_2O) and carbon dioxide (CO_2). These volatiles play a crucial role in every facet of life. An example includes taking centre stage as the key building blocks for life on Earth and H_2O also has a profound impact on plate tectonics, where it is largely responsible for its geotectonic mobility. Subduction zones are one of the major sites of volcanism on the Earth. A significant amount of H_2O alongside CO_2, is expelled from the subducting slab and contributes significantly to melt generation. Interestingly the main hydration event for the oceanic plate takes place at the trench during bending-related deformation. The amount of water stored in the upper lithosphere appears to be strongly dependent on the plate curvature, bending moment and slab dip; the plate age controls the maximum depth at which water can percolate. The ability of oceanic plates to deliver chemically bound water at depth depends on the slab thermal regime. Hot slabs dehydrate fast while in very cold slabs, oceanic crust dehydration completes at a maximum depth of 300 km (Figure 4.12). The release of water plays a major role in the genesis of magma and metamorphism in subduction zone environments, which are likely to be related to the growth of continents and orogeny on geologic time scales. The majority of arc magmas appear to be derived from partial melting of the mantle wedge induced by lowering the mantle solidus by upward infiltration of fluids released from the dehydrating slab. This results in cooling of the fore-arc region, as expressed by the low surface heat flow (<40 mWm^{-2}) observed at many fore-arcs and as indicated by the inferred existence of serpentinite and chlorite in the sub-arc regions, which are stable only below 700°C. Melting might be initiated at the vapor-saturated solidus near the base of the wedge at high pressure. The H_2O-rich melt that is initially produced continuously reacts with overlying hotter, shallower

mantle, diluting the magmatic H_2O content as the melt ascends. Arc-related igneous rocks display a typical trace element abundance spectrum, the so-called 'arc-signature', characterized by the enrichment of highly mobile large ion lithophile elements (LILE) relative to high field strength elements (HFSE). This signature can be explained by a two-component mantle source consisting of variably depleted asthenospheric mantle and a hydrous fluid (or H_2O-saturated low percentage melt) that originates from the breakdown of hydrous phases transported in the cold part of the partly hydrated oceanic lithosphere. The principal effect of H_2O on the partial melting is a reduction of the melting temperature by 100–150°C for moderate to substantial amounts of partial melting (10–25 wt. %) compared to anhydrous melting of a lherzolite source. Such a reduction of the melting temperature requires the presence of 0.1–0.5 wt. % H_2O in the source and results in 1–7 wt. % H_2O in the basaltic to picritic primary liquid. The majority of primitive arc magmas are basaltic and do not represent near-solidus H_2O-saturated liquids that are highly alkalic and mostly nepheline-normative. The decrease of the melting temperature on the order of 100–150°C compared to anhydrous peridotite melting requires high melting temperatures of 1250–1300°C at 1.5 GPa (45 km depth) and 1350–1400°C at 2.5 GPa (70 km depth) that are close to the average current mantle adiabat (ACMA). Therefore, partial melting in the mantle wedge is confined to the hottest region where temperatures approach undisturbed asthenospheric conditions. At a given pressure (depth) hydrous melts are less magnesian and more silica-rich than melts produced under anhydrous conditions. Arc magmas (and their mantle sources) are more oxidized than MORB or OIB melts (and their respective mantle sources).

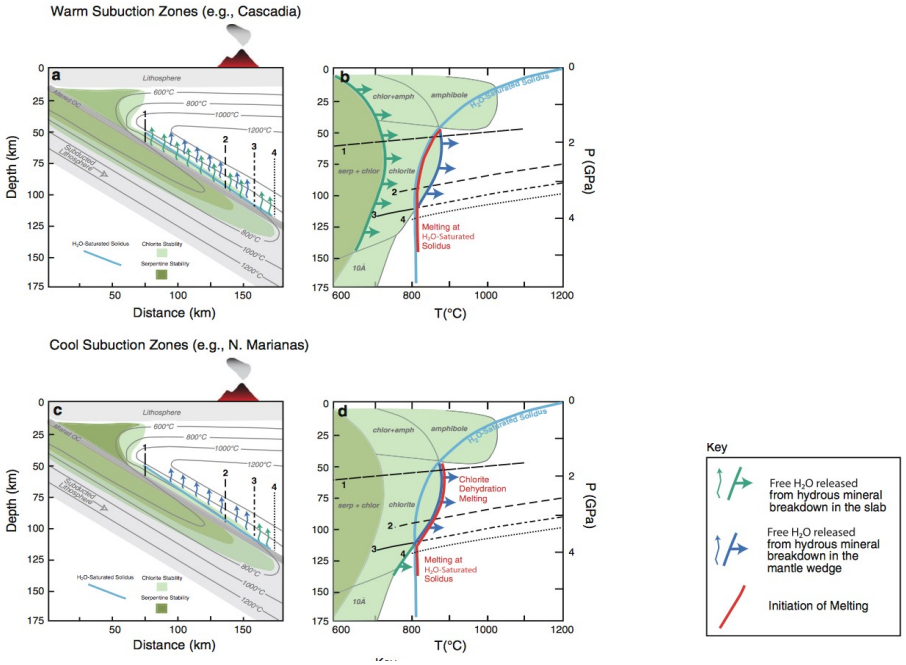

Figure 4.12. Diagrams of the location of H_2O release and the initiation of melting in the mantle wedge below volcanic arcs. a and c: cartoons of the mantle wedge illustrating chlorite and serpentinite stability and the location where the breakdown of these hydrous phases produces free H_2O available to trigger H_2O-saturated melting in the mantle wedge. b and d: hydrous under-plating peridotite phase diagrams illustrating the location where the breakdown of the hydrous phase produces free H_2O able to trigger H_2O saturated melting in the mantle wedge. At warm subduction zones, the quantity of H_2O fluxed from the slab at subarc depths is greater than that which can be bound in a 1 km thick layer of the chloritized peridotite at the base of the mantle wedge

and will therefore trigger melting at the temperature of the H_2O saturated solidus. The dehydration of chlorite in the mantle wedge will promote ongoing H_2O saturated melting. In the cold subduction zones, the lesser quantity of H_2O fluxed from the slab at subarc levels can be bound in a 1.5 thick layer of chloritized peridotite and melting will not occur until the P-T conditions for chlorite dehydration are reached. (From Till et al. 2012).

Volatile recycling in subduction zones, especially H_2O, greatly affects the physicochemical properties of the overlying mantle wedge. As the mantle wedge hydrates, it loses its strength, density and viscosity are considerably reduced, and the depleted mantle undergoes hydration induced flux melting. On the other hand, the physicochemical effects of metasomatism with a carbonic fluid remain subtle and enigmatic. The fluid typically precipitates an accessory phase (i.e., carbonate, graphite, or diamond) during interaction with a depleted peridotite. CO_2 also decreases the solidus temperature of peridotites, eclogites, and sediments. Subduction zone melting typically releases hydrous silicate melts, and in some rare cases experiences high enough temperatures to initiate carbonatitic melting. The resultant melts are extremely mobile and have low viscosities. The melts may also extract incompatible, heat producing elements (i.e., U, Th, and K). Carbonate melt impregnation and element scavenging can locally influence the long term heating budget of the metasomatised mantle portion, resulting in localized thermal anomalies that may occur at different depths of the upper mantle. Furthermore, carbon is economically significant, important in its elemental form as either diamond or graphite. Carbonatite complexes (rare igneous intrusives primarily consisting of carbonate) are also a major source of rare earth elements (REE). Most importantly, the global carbon cycle and habitability of our planet greatly depend on carbon stability and residence time in the mantle, recycling efficiency in subduction zones, and rates of magmatic degassing.

4.4.1. Production of CO_2.

The cycling of carbon into and out of the mantle is a fundamental, yet largely unconstrained problem in the geosciences, typically overshadowed by the study of deep subduction of water into the mantle. However, over the past two decades, there have been several key reviews that estimate the amount of CO_2 or elemental carbon recycling at convergent and divergent margins. Indeed, there are many scientific studies, some involving experiments over a vast array of disciplines, in an effort to gain better insight into volatile recycling. For example, volcanic gas monitoring brackets the amount of slab derived carbon versus mantle carbon degassed during arc volcanism, experimental approaches have determined the solidi of subducting components and their corresponding melts, and thermodynamic modeling has placed theoretical limits to decarbonation. However, the overarching conclusion of the community is that they were unable to reconcile the source and mechanism by which CO_2 fluxes were generated at subarc depths observed by volcanic gas monitoring. This has led to the so-called CO_2 deficit, where present day subduction geothermal gradients remain too low for efficient carbonate removal from the down-going slab. The idea of a CO_2 deficit, however, has been recently challenged by Kelemen and Manning (2015), where new thermodynamic data coupled to field observations suggest it is

possible that carbon can be efficiently removed through different subducting mechanisms and stored in the lithosphere as opposed to being recycled into the convective mantle.

Carbon input into the mantle is dependent on three important geochemical reservoirs entering the subduction trench. First, alteration of oceanic basaltic crust is the largest contributor with 22-29 Mt C/year. The carbon concentration in altered oceanic crust is typically age dependent and is an alteration by-product of hydrothermal activity at mid-ocean ridges. Carbon is typically fixed within carbonates that exist as vugs and veins within the crust as opposed to a pervasive alteration. Sediments are the second largest contributor ranging between 13-23 Mt C/y. However, sediments are the most variable carbon contributor because fluxes are constrained by environmental conditions and subduction type (i.e., intra-oceanic, continent-continent, or oceanic-continent). These external variabilities may manifest as non-steady state carbon fluxes through time. Last, carbon uptake at the outer rise (4-15 Mt C/y) may constitute a significant proportion of stable carbon input into the subducting lithospheric mantle. The outer rise is a consequent result of oceanic plate bending prior to subduction. Slab bending results in focused lithospheric cross-cutting faults and has been seismically correlated to serpentinisation. However, this estimate is uncertain due to a lack of constraints on the extent of serpentinisation at the outer rise.

Table 4.1. Estimates of the carbon budget in the lithosphere-subduction-atmosphere system.

Tectonic setting	Mt C/yr	
	Min	Max
Carbon input into subduction zones	40	66
Total output from subduction	14	66
Output to atmosphere	18	43
Diffuse output to ocean and atmosphere in arc systems	4	>12
Storage in shallow mantle	0	47
Subducted carbon into convecting mantle	$1x10^{-4}$	52
Output to ocean and atmosphere at ridges and ocean islands	8	52

4.4.2. Hydration and carbonation reactions.

Metamorphic reactions (dehydration and decarbonation) result in the release of H_2O–CO_2 fluids. These reactions occur due to changes in the pressure, temperature, and the breakdown of stable minerals. In subduction zones, the primary hosts for volatile release in fore-arcs are typically pore fluids within sediments and altered basalts. Volatile reservoirs can exist to sub-arc depths and beyond as structurally bound volatiles (commonly called the alphabet phases) within hydrous and carbonated minerals depending on the subduction style and thermal structure of the slab. Understanding devolatilisation reactions is of great importance because released fluids affect the evolution of the subduction zone via weakening of the overlying mantle wedge and the long term regulation of water and carbon budgets on Earth.

Implementation of petrological components (i.e., metamorphic and solid-state phase changes, melting, melt extraction, and geochemical fractionation) into geodynamic numerical

models has been a critical area of advancement and research in the understanding of ongoing processes within Earth. For example, mantle convection codes were the first numerical models to implement petrological components. The objective was to better understand the response of global mantle convection models due to the effect of solid-state phase transitions (e.g., olivine → wadsleyite) in contrast to the standard thermal convection (Rayleigh-Benard) and subduction models. Major phase changes were originally programmed manually by using Clapeyron slopes. However, the proliferation of thermodynamic modeling tools (e.g., Perple X and Thermocalc) led to a revolution in geodynamic modeling techniques. Automated strategies for thermodynamic calculations led to more advanced and accurate geochemical implementations by coupling melting processes, seismic properties, and dynamic density calculations. The so-called petrological-thermomechanical models are now included in many codes and are applied to different geodynamic problems.

The petrological models (Figures 4.13 and 4.14) in this chapter are the product of synthetic thermodynamic modeling. Thermodynamic modeling is a very powerful tool that allows us to predict stable phases from the bulk compositions of commonly subducting rocks (Table 4.2) at convergent zones. We can extract important information, such as seismic data, density, and even melt proportions as a function of different thermodynamic variables. As we are interested in the devolatilisation of water and CO_2, we first want an understanding of how the fluid availability changes with pressure, temperature, and stable phases (Figures 4.13 and 4.14).

We generated pseudosections for GLOSS average sediments (a globally average composition for convergent margins) and extracted thermodynamic properties via Perple X, superimposing the information onto one another to highlight how phase boundaries control volatile concentrations (Figure 4.13 a–c). The models focus on relevant pressures (0.05-7 GPa) and temperatures (300-1500°C) to devolatilisation in subduction zones. We highlight the major volatile phase boundaries and consequent changes in CO_2 wt. % and H_2O wt. % due to discontinuous reactions (e.g., lawsonite; Figure 4.13 a).

Our models show that carbonate is relatively stable in sediments (Figure 4.13 a), similar to others that have predicted little decarbonation. The continuous gradations of the carbonate phases and relatively stable CO_2 wt. % as fluid, as opposed to the breakdown of chlorite, amphibole, and lawsonite (Figure 4.13 b), means that carbonates resist decarbonation in nearly all but the hottest subduction zones. This is because subduction paths typically take sub-parallel slopes to the carbonate-out reactions. However, as carbonates are particularly sensitive to temperature changes (i.e., a steep Clapeyron slope), decarbonation may only be attainable in specific subduction cases where low pressure – high temperature scenarios exist, such as sedimentary diapirism (Figure 4.15).

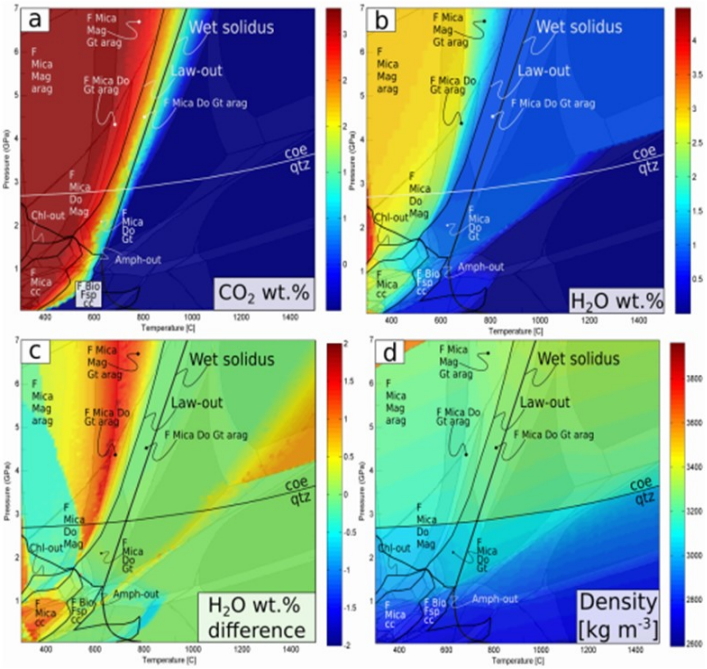

Figure 4.13. Pressure-temperature diagrams for GLOSS average sediments. Pseudosections are calculated via Perple X and superimposed with extracted thermodynamic properties. Sediment compositions and thermodynamic phases taken from Table 4.2 . Wet solidus for sediments after Poli and Schmidt (2002) and Schmidt and Poli (1998). Major hydrous phase boundaries for lawsonite, chlorite, and amphibole are marked. Metastable, immiscible phases, and phases beyond solidus omitted for clarity. Omph is present in all phase fields. Abbreviations used in all pseudosections: F-fluid; coe - coesite; qtz - quartz; Mica - white mica; Gt - garnet; Mag-magnesite; arag - aragonite; Do - dolomite; cc - calcite; Chl - chlorite; law - lawsonite; Fsp - feldspar; Opx -orthopyroxene; Omph - omphacite; Amph - amphibole; Bio - biotite; O - olivine; phA - phase A; Atg - antigorite; Sp - spinel. (a) CO_2 wt. % derives from a combination of CO_2 in fluid and carbonates. CO_2 remains within solid carbonate and resistant to decarbonation. (b) H_2O wt. % as a combination of water in fluids and mineral bound phases. (c) Calculated difference in H_2O wt. % between the old and new look–up tables. (d) Extracted density of the sediments (kg m^{-3}).

Table 4.2. New and old (H_2O only) bulk oxide wt. % compositions for representative subducting lithologies. Sediments are GLOSS average sediments (Plank and Langmuir, 1998), metabasalts from Staudigel at al. (1989) and Gerya et al. (2006). Mantle values are taken as the LOSIMAG average after Hart and Zindler (1986). The LOSIMAG composition is altered to account for CO_2.

Oxides	***Sediments***		***Oceanic Crust***		***Mantle***	
	New	**Old**	**New**	**Old**	**New**	**Old**
SiO_2	58.57	61.10	46.6	47.62	44.05	45.55
Al_2O_3	11.91	12.43	15.26	14.48	4.03	4.03
FeO	5.21	5.43	9.84	10.41	7.47	7.47
MgO	2.48	2.59	6.54	6.92	37.42	37.42
CaO	5.95	6.21	12.66	13.39	3.18	3.18
Na_2O	2.43	2.54	2.03	2.15	0.33	0.33
K_2O	2.04	2.13	0.55	0.58	0.03	0.03
H_2O	7.29	7.60	2.63	2.78	1.98 (MAX)	1.98 (MAX)
CO_2	3.01	-	2.9	-	1.5 (MAX)	-

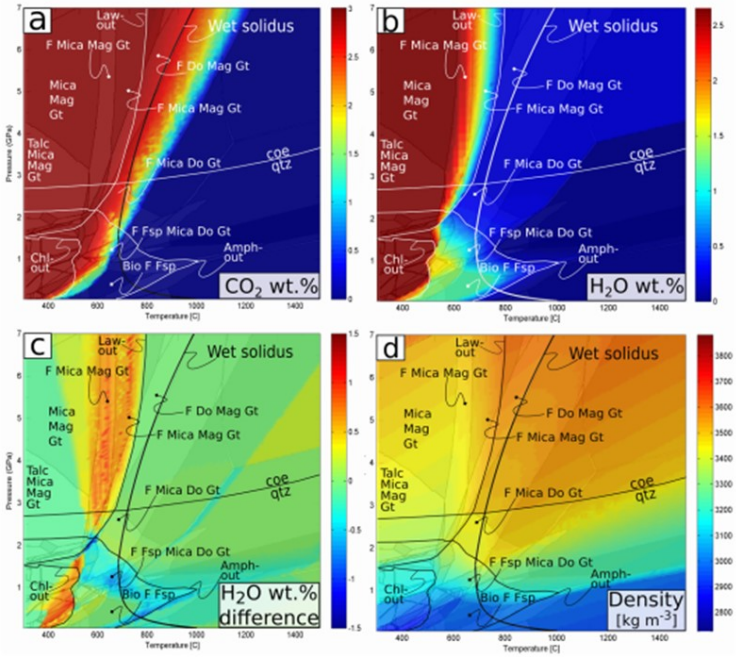

Figure 4.14. Pressure-temperature diagrams for altered carbonated basalts. Pseudosections are superimposed with extracted thermodynamic properties. Bulk compositions and thermodynamic phases taken from Table 4.2. Wet, CO_2–absent solidus for hydrated basalt after Schmidt and Poli (1998). Major hydrous phase boundaries for lawsonite, chlorite, and amphibole are marked. Metastable, immiscible phases, and phases beyond solidus omitted for clarity. Cf. Figure 4.12 for phase abbreviations. (a) CO_2 wt. % derived from a combination of fluid and carbonates. CO_2 remains within solid carbonate and resistant to decarbonation. Decarbonation beyond the wet solidus, except low temperatures. (b) H_2O wt. % as a combination of water in fluids and mineral bound phases. (c) Calculated difference in H_2O wt. % between the old and new look–up table. Calculated by subtracting the difference between old and new look–up table. (d) Extracted density for altered basalts.

4.4.3. CO_2 and subduction.

Subduction of heterogeneous lithologies (sediments and altered basalts) carries a mixture of volatile components (H_2O-CO_2) into the mantle, which are later mobilized during episodes of devolatilisation and flux melting. Volcanic gas monitoring and melt inclusions attest to the presence and transfer of carbon during subduction into the overlying mantle wedge. CO_2 is the second most abundant volcanic gas with concentrations averaging between 2500 and 7600 ppm in arcs and reaching maximum concentrations up to 0.4-1.7 wt. % (based on Mount. St. Helens melt inclusions). Furthermore, it has been shown that sediments, carbonate limestones, and organic matter contribute the majority of carbon output in arc volcanism with the remaining 20% of carbon derived from a MORB-type source. In addition, field observations in HP-UHP terranes demonstrate the presence of carbonic fluid across the slab-mantle wedge interface, where carbonated peridotites and eclogites as well as microdiamond and graphite are detected. In contrast, studies of decarbonation reactions show the amount of fluid released as a function of P-T tends to decrease CO_2 in the system as it slowly partitions into carbonate minerals (i.e., dolomite and magnesite). Carbonate partitioning occurs at pressures >2 GPa with minor decarbonation at forearc depths derived from subducting

oceanic sediments. Therefore, according to both thermodynamic and experimental investigations decarbonation at subarc depths should be limited. Subsequently, a calculated carbon deficit exists between the amount of carbon recycled and the amount of carbon returned to the surface via degassing. Three geodynamic regimes show significant decarbonation. (i) Sediment diapirism acts as an efficient physical mechanism for CO_2 removal from the slab as it advects into the hotter mantle wedge (Figure 4.15). (ii) If subduction rates are slow, frictional coupling between the subducting and overriding felsic crust occurs. Mafic crust is mechanically incorporated into a section of the lower crust and undergoes decarbonation (Figure 4.16). (iii) During regime (extension-compression) within subduction the amount of degassing changes (Figures 4.15, 4.16 and 4.17).

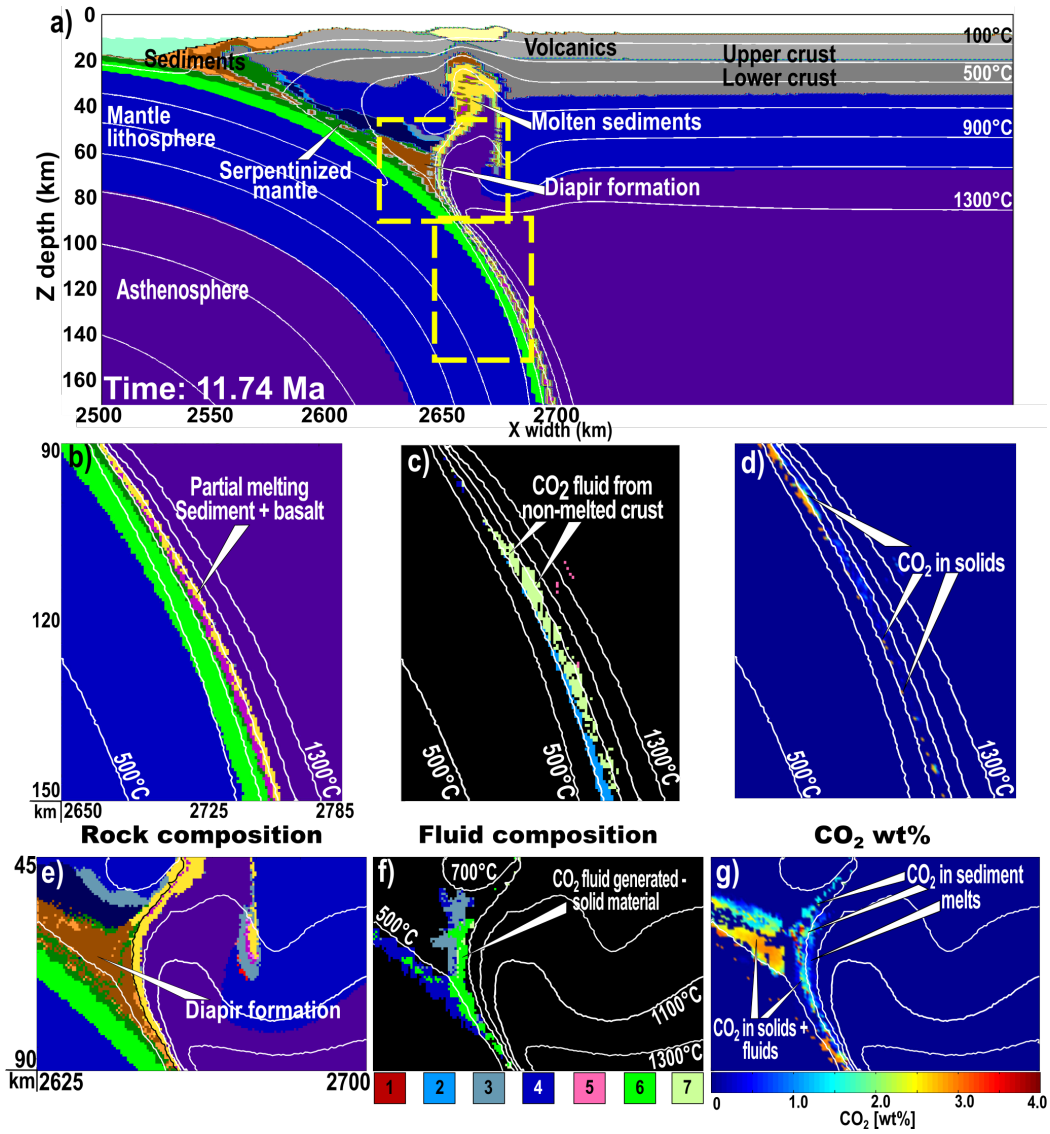

Figure 4.15. Model development for a trans-lithospheric diapir. (a) Snapshot of full model at 11.74 Ma. (b) - (d) Enlarged images of slab surface at depth. (e) - (g) Enlarged image of diapir formation. Panels (e) - (f) illustrate the development of CO_2 transportation via melt solubility in sediments (g) and fluid generation in sediments just below the 700°C isotherm. (b) and (e) Rock composition. (c) and (f) A fluid map, which visualizes the release of free fluids in the model. Colored boxes and respective numbers are representative of the fluid generated

from rock (i) H_2O fluid generated from peridotite, (ii) H_2O fluid generated from gabbros, (iii) H_2O fluid generated from sediments, (iv) H_2O fluid generated from altered basalts, (v) CO_2 fluid generated from a carbonated peridotite, (vi) CO_2 fluid generated from sediments, and (vii) CO_2 fluid generated from carbonated basalts. (d) and (g) Concentration of CO_2 wt.% stored in rocks, fluids and molten sediments. (d) CO_2 is subducted to the deeper mantle in solid basalts that have not undergone partial fusion. (Figure provided by C. Gonzalez)

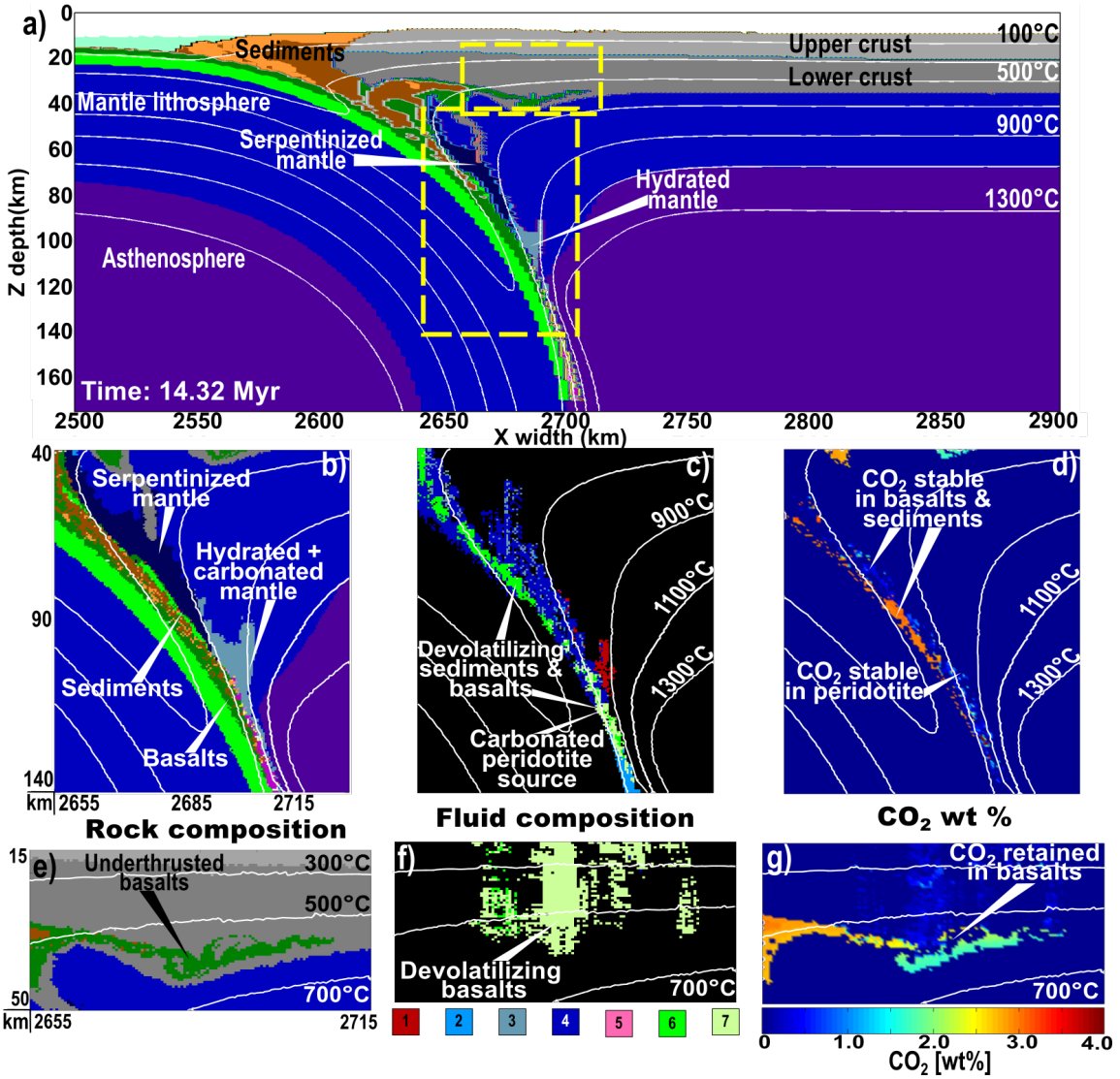

Figure 4.16. Panels (a) - (g) represent a snapshot in time at 14.32 Ma for an under-thrusting basalt. Yellow boxes represent an enlarged view. Smaller yellow box represents enlarged view of the under-thrusted component. Larger yellow box represents enlarged view of the slab surface. (a) An overall compositional snapshot of the subduction zone. (b) - (d) Enlarged view of the slab surface at depth. (e) - (f) Enlarged view of basalts in the lower crust (b) & (e) rock composition. Panels (c) & (f) are a fluid map, which visualizes the release of free fluids in the model. Each color corresponds to its derivative lithology (cf. Figure 4.15 for color and rock associations). (d) and (g) Concentration of CO_2 wt. %. Concentration is representative of CO_2 in fluids, solids, and sediment melts. This model represents the development of a young slab colliding with the continental crust and under-scraping basalts. (f) Low pressure and higher temperatures results in decarbonation of altered basalts. Panels (b)-(d) illustrate decarbonation in the forearc of sediments and basalts as well as the carbonation of peridotites (c)-(d). (Figure provided by C. Gonzalez)

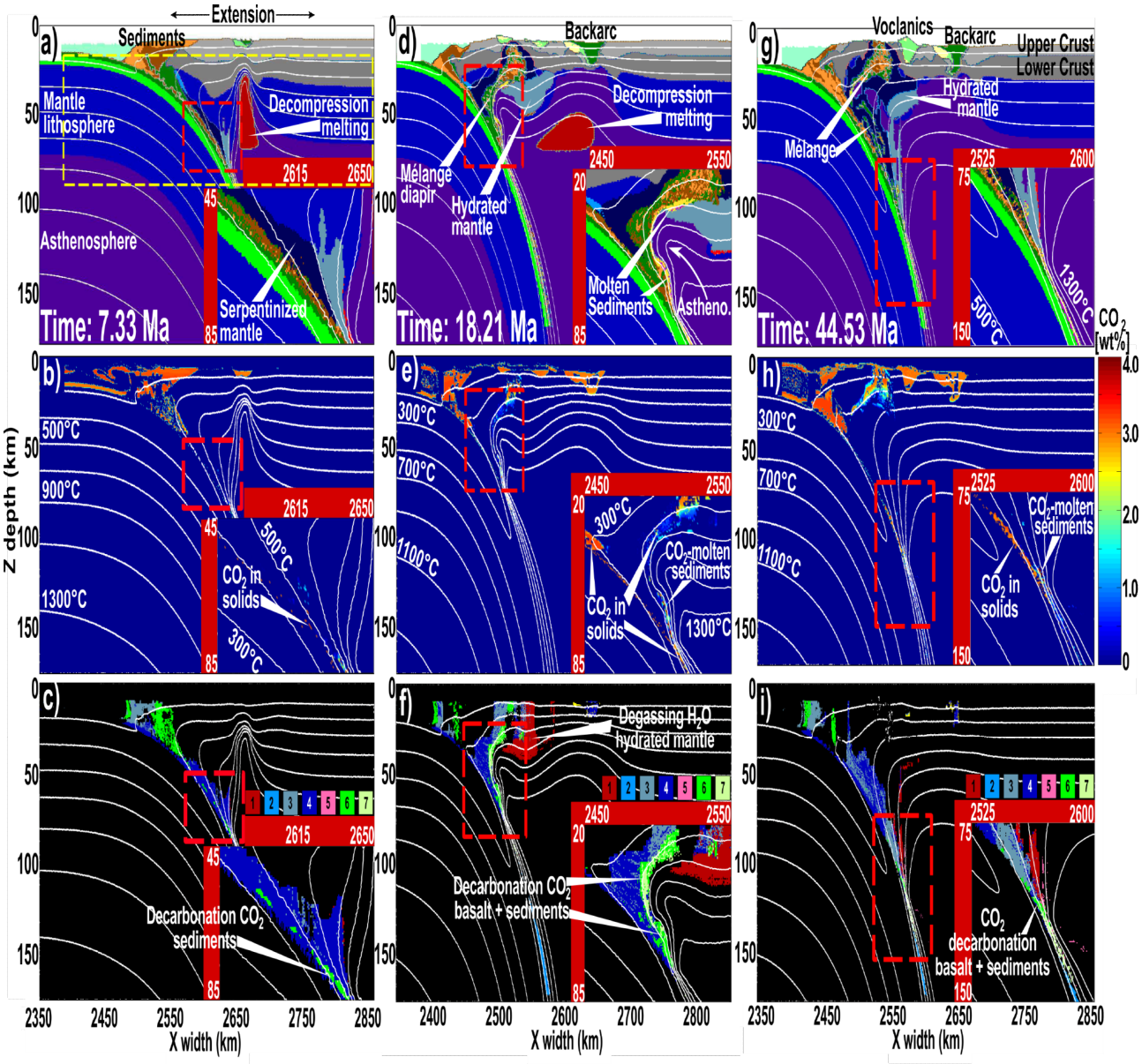

Figure 4.17. Model development for irep80 showing how dynamics of subduction can lead to decarbonation. (a), (d), and (g) are compositional time slices at 7.33 Ma, 18.21 Ma, and 44.53 Ma. Red dashed box highlights an enlarged portion in the corner of the model box. (a) Extension initiation, (b) end of decarbonation peak and waning stages of the extensional event, and (c) onset of stable subduction. Yellow dashed box highlights area in which CO_2 fluxes are calculated (Figure 4.17a). (b), (e), and (h) Concentration of CO_2 wt. % stored in rocks, fluids and molten sediments. Panels (c) and (f) are a fluid map, which visualizes the release of free fluids in the model. Each color corresponds to its derivative lithology (cf. Figure 4.15 for color and rock associations). This model illustrates the importance of including dynamics when considering decarbonation in subduction zones. Without the heat from the asthenosphere fluxing in, decarbonation fluxes would be minimal.

4.4.4. Subduction and orogenic gold mineralization.

In order to emphasise the importance of slab roll-back in the production of CO_2 and H_2O coupled to orogenic gold mineralisation we zoom into part of Figure 4.17 at 18 Ma in Figure 4.18 (a). CO_2 and H_2O are released from the slab over a limited amount of time (≈ 5 my) when the slab rolls back and higher thermal gradients are experienced in the melange material at shallow depths. In this case, the CO_2 released in high quantities can be considered

a '*one-off*' event. In terms of pure decarbonation, the carbonates never reach a sufficient temperature along the slab surface to break down under normal, or non-rollback conditions. Decarbonation typically occurs in sediments at subarc depths (e.g., >40 Ma), but never in such a way that is significant volumetrically. Figure 4.18 (b) shows that the release of CO_2 in the period ≈ 15 Ma to ≈ 18 Ma coincides with a period of extension and is almost 1000 times higher than background before the event reaching ≈130 kg m^{-3}. This CO_2 release coincides with a maximum in H_2O release (Figure 4.18 c).

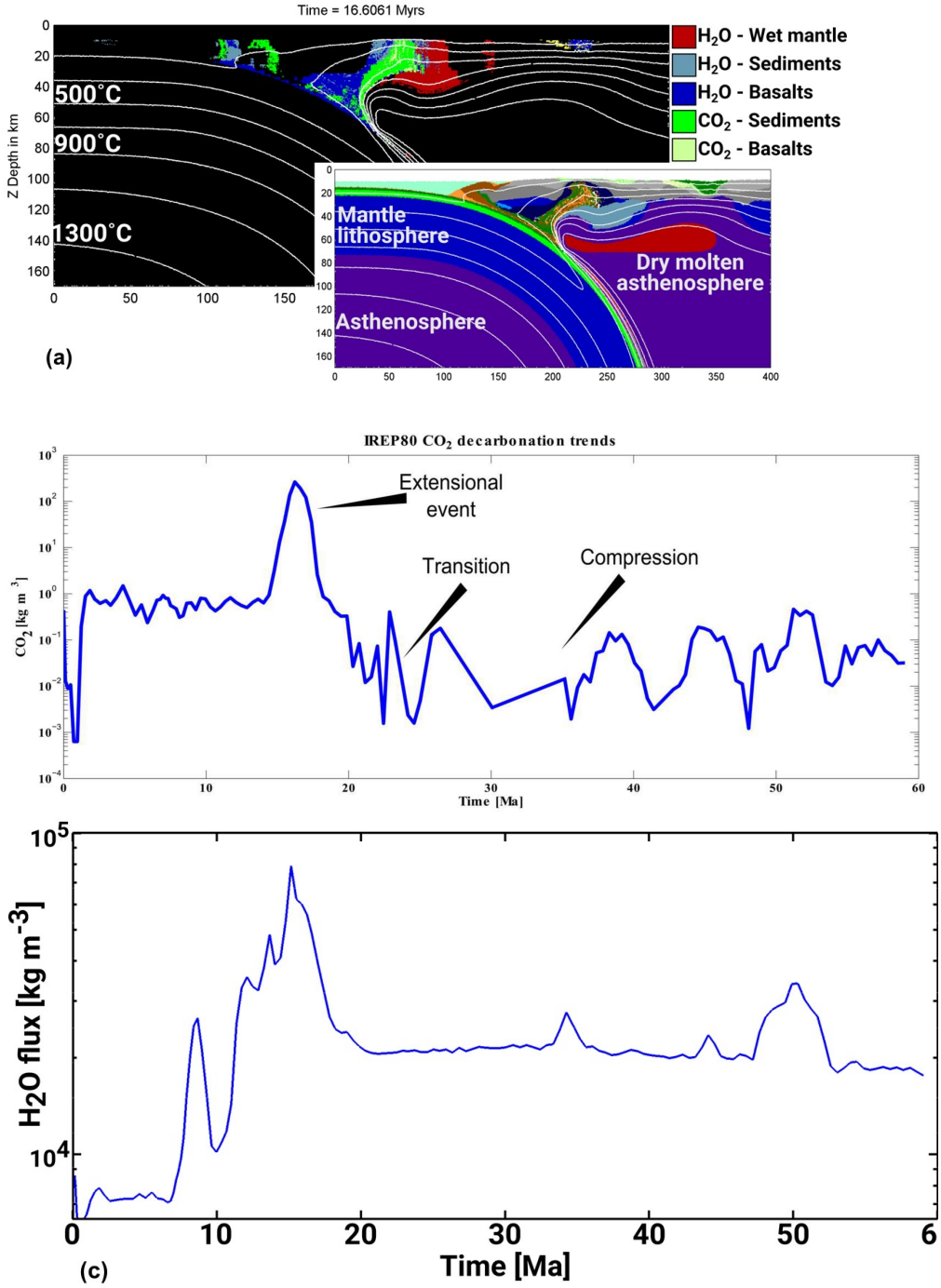

Figure 4.18. Release of CO_2 and H_2O over a short period of time (≈ 3 my) during a roll-back event. (a) The model at the time of roll-back. Hot asthenosphere intrudes into a position near the down-going slab so that a plume of CO_2 is generated for a short period at rollback before the asthenosphere relaxes

thus cooling the slab. (b) CO_2 flux time series calculated for model irep80. Fluxes are calculated based on fluid release and whether or not that fluid marker moves toward the surface within the next time step. If so, the fluid marker is counted and will no longer be counted afterwards. Log plot shows the order of magnitude increase of decarbonation during the extensional period over the late stable subduction regime. (c) H_2O release as a log plot for the same model.

4.4.5. CO_2 and rifting.

Another interesting aspect of CO_2 cycle is non-volcanic CO_2 degassing and in intra-continental settings, and its source during extensional events. Mantle CO_2 degassing is currently a topic of debate and whether it is passive or volcanic related. Continental rifts, such as the East African rift, have been shown to experience non–volcanic CO_2 degassing that has largely been in the past. Recent gas probe chromatography has shown that upper-mantle degassing off-rift axis may be an important and largely underestimated component in global, naturally occurring source of CO_2 fluxes. Other continental rifts, such as the North Atlantic Craton, have experienced a unique suite of volcanic rocks, such as ultramafic lamprophyres, carbonatites, and mafic alkaline rocks often attributed to carbonate metasomatism in the SCLM. Understanding these sources from a geodynamic point of view is not only an important factor in our global carbon cycle, but also important from a seismic hazard point of view. Here we will show the role of a carbonate metasomatised SCLM and the release of CO_2 fluid in proximity to ongoing rifts. We found three different rifting regimes that were dependent on the amount of time the model was subjected to extension: (i) Failed rift without any CO_2 decarbonation, (ii) failed rift with CO_2 decarbonation, and (iii) semi-failed rift that experienced asthenospheric melting.

Failed rift with CO_2 decarbonation

In failed rifting examples, we observe a short–lived, CO_2 flux (Figure 4.19) situated in the middle of the model with an arch–like geometry. This is followed by a sharp decline in CO_2. After 14.2 Ma there is no CO_2 flux. This burst of CO_2 lasts for ≈ 4.2 my and the maximum volume is higher than in the subduction case at $\approx 10^{5.5}$ kg m^{-3}. This clearly is a very attractive scenario for orogenic gold mineralization and relies on the rifting at the site of previously metasomatised lithosphere.

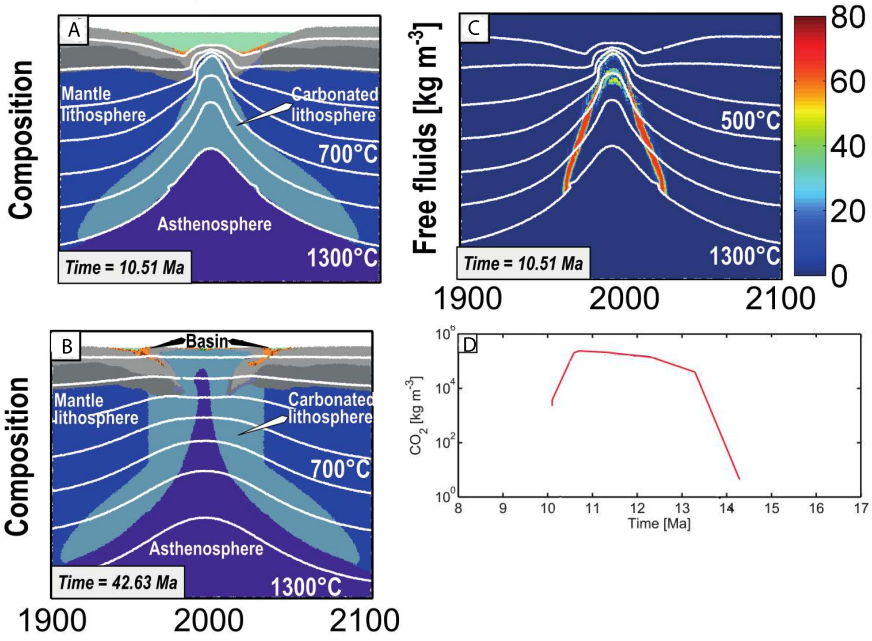

Figure 4.19**.** Snapshot shows a failed rift with decarbonation. (A, B) – Rock composition - (A) during CO_2 release, (B) after release of CO_2). (C) Free fluid (CO_2) flux during rifting, showing an arch–like geometry . (D) CO_2 flux through time. CO_2 flux that lasts 4.19 Ma.

Semi-failed rift.

Semi-failed rifts are characterized by the sustained presence of an asthenospheric melt during extension. CO_2 flux (Figure 4.20) shows a downward trend. However, as total flux decreases, the duration of fluxes increase. We see here focusing of fluids beneath the rift axis in the first 10 Ma and subsequently transitioning to the flanks of the rifted margins toward the end of the model runs. The maximum flux is again high at $\approx 10^4$ kg m^{-3}.

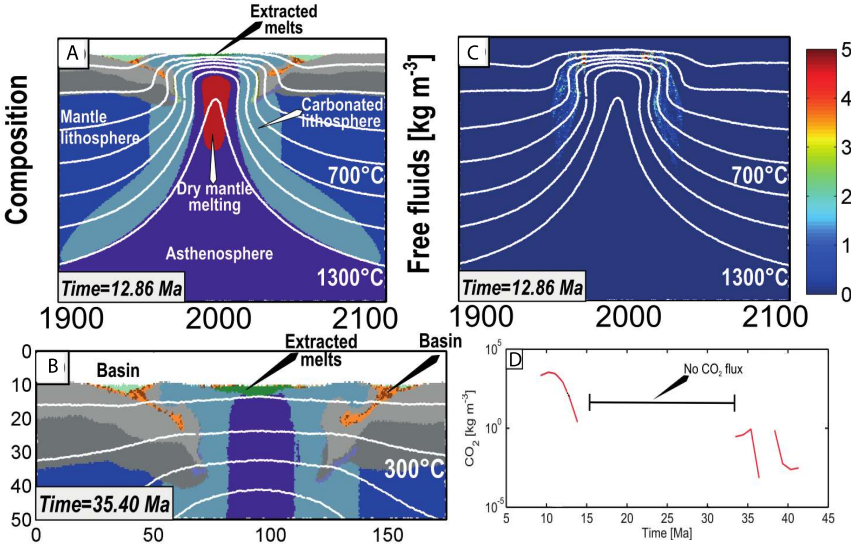

Figure 4.20. Snapshot shows a semi-failed rift with decarbonation. (a–b) – Rock composition - (a) during first episode of CO_2 release, (b) during second episode of CO_2 release). (c) – Free fluid (CO_2)

flux during rifting, shows the nature of fluids degassing along the rifting margin edges. (D) – CO_2 flux diagram illustrating early (~9 Ma), pulse of CO_2 flux. Flux is short lived and quickly decrease in magnitude. Second very small flux occurs after 36Ma.

4.5. CO_2 from regional metamorphic crustal sources.

Phillips and Powell (2010) present a case for CO_2 release from mafic rocks in the crust resulting from the transition from greenschist to amphibolite regional metamorphism. Clearly the results of such devolatilisation will resemble those arising from devolatilisation of a subducting slab (Figure 4.18) or from rifting scenarios (Figures 4.19 and 4.20). The essential differences are:

- The regional metamorphic devolatilisation system is likely to have a greater spatial extent than the rollback subduction or rifting systems. The subducting devolatilizing system scenarios clearly produce potential mineralisation sites restricted to the margins of the rifts, restricted to a stripe perhaps 100 km wide and a few 100's of kilometers long; the rifting crustal system may have a broader distribution. In this regard the Victorian goldfields perhaps have a crustal regional metamorphic origin for CO_2.
- The rates at which CO_2 is released differ for the subduction/rifting as opposed to the regional metamorphic systems by perhaps two orders of magnitude. The release rate for the crustal devolatilisation system depends on the rate at which the isotherm corresponding to the greenschist/amphibolite transition rises in the crust. In particular the total rate of generation of fluid, Q, in the reaction zone (volume per unit time per unit area of the devolatilizing zone) is given by

  $$Q = n_{fluid} V U s_0$$

  where n_{fluid} is the number of moles of fluid released by one mole of the devolatilizing mineral, V is the molar volume of the fluid at ambient temperature and pressure, U is the rate at which the reaction front moves through the equilibrium devolatilisation isotherm and s_o is the number of moles of the devolatilizing mineral in the unreacted material. If the movement of the devolatilizing assemblage through the equilibrium reaction isotherm occurs solely by thermal conduction then the rate of isotherm rise is of the order of 1mm y^{-1} (see Figure 2.13 b). In the subduction/rifting cases the rate of CO_2 release is controlled by the rate at which the subducting slab passes through the P-T conditions where CO_2 is released or by the rate of rifting. This is likely to be of the order of 50 – 100 m y^{-1}. Thus the spike in CO_2 release in Figure 4.18 lasts for 3 my and that in Figure 4.19 (d) lasts 4.2 my whereas release of CO_2 from a regional metamorphism event is likely to last at least 30 my.
- Maximum fluxes of CO_2 in the subducting system are closely related to distinct changes in the tectonic regime associated with slab roll-back. Regional metamorphism is much more extended in time and associated with many deformation events rather than a short lived extensional event as recorded in Figure 4.18.
- Maximum fluxes in the rifting scenarios (Figures 4.19 and 4.20) are clearly related tectonically to rifting events whereas regional metamorphism is much more extended in time and associated with many deformation events

Otherwise, the various origins for CO_2 share similar characteristics. All source the fluids and the gold in the same rock sequence, both develop H_2O, H_2S and CO_2 at the same time (a requirement according to Phillips and Powell (2010) for the production of auriferous fluids) and all deliver volumes of fluid sufficient to produce high grade ore deposits. The difference in regard to regional metamorphic origins is that the subduction/rifting systems deliver these volumes of fluid in a much more focused manner both spatially and temporally than a regional metamorphic model.

4.6. Archean tectonics.

Geologists have long debated the timing of the onset of plate tectonics on Earth. There has been a consensus that as Earth cools, tectonic activity will wane and eventually Earth will settle into a cold, stagnant-lid regime, similar to Mars today. However, there is no such consensus on what form tectonics on the pre-plate tectonics early Earth might have taken. The only contemporary example for a hot interior rocky body is tidally-heated Io, which exhibits a stagnant tectonic regime with extreme volcanic resurfacing; a sub-regime known as a "heat-pipe" stagnant lid regime.

This debate has extended into exo-solar planets, with arguments for and against the likelihood of active tectonics on larger super-earths. One of the ambiguities in the debate is the extent to which the heating mode affects surface stresses and tectonic regime. Simple scaling theories, based on basally heated convection, demonstrate increased convective stresses with increasing Rayleigh number – which, in isolation, translates to higher lithospheric stresses for larger planets. However, increases in internal heating rate for a given planet's size has also been shown to be able to cause a transition from mobile lid convection, into an episodic regime, and eventually into stagnant lid convection. It has been demonstrated that the scaling for mixed heating thermal convection can be quite different than for purely basal heated cases, though these are models without a tectonically active surface. The balance between basal heating, internal heating, and secular cooling has not been adequately mapped with reference to tectonic regime.

Box: Stagnant lid convection.
Stagnant lid convection is a form of convection that occurs in a material with strongly temperature dependent viscosity for a viscosity contrast larger than about 104. It is characterized by an upper stagnant layer – the stagnant lid – that forms on top of the convecting layer. Heat in the stagnant lid is transported mainly by heat conduction. Stagnant lid convection is typical of mantles of the terrestrial planets, Mercury, Mars and Venus and large rocky satellites such as the Moon. Stagnant lid convection may also occur in the ice layers of the icy satellites of the outer Solar System. Stagnant lid planets are usually also one-plate planets. Their tectonic style differs substantially from planets with mobile lid convection or plate tectonics like Earth. Here, the near-surface layers take part in the convective flow and are recycled with the interior.

There seems to be a consensus emerging that plate tectonics as we know the concept today began at about 3 Ga (see Chapter 2) with two significant events after 3 Ga namely, a whole mantle overturn resulting in widespread mafic volcanism at 2.8 Ga and the perovskite post-perovskite transition at 2.3 Ga. In the absence of forces generated by subduction the only forces acting on the lithosphere are gravity and surface tractions arising from mantle convection on the base of the lithosphere. In addition in the absence of heat loss at mid-ocean ridges the only dominant modes of heat loss from the Earth are conduction (with subsequent radiative heat loss to space) and intrusion of hot mantle into the lithosphere with subsequent loss of heat from the solidifying magma arising from the latent heat of crystallisation. This latter process resembles the action of a heat pipe whereby heat is lost from the system via a phase transition. In this instance heat transfer is by advection whereas in many commercial heat pipes heat transfer is by conduction. We refer to this process below as a heat pipe mechanism.

With these observations in mind the following three modes of deformation are possible:

- The lithosphere can fail by acceleration instabilities (see § 4.2.2) usually identified as Rayleigh-Taylor instabilities whereby a heterogeneity in mechanical properties or density initiates a gravitational instability that results in detachment of part of the lithosphere into the mantle and subsequent upwelling of hot mantle and decompression melting, emplacement of intrusions and generation of surface volcanism. This process constitutes a particularly complicated heat pipe but nevertheless is an efficient mechanism for losing heat from the Earth. This process is also a way of increasing the overall thickness of the crust and of transporting radiogenic isotopes into the crust.
- The lithospheric basal traction on the lithosphere generates a region of horizontal shearing through the lithosphere (Figure 4.21 a, b) expressed as lozenge shaped regions of weakly deformed material enclosed in an anastomosing network of shear zones (Figure 4.21 a, b) This process occurs synchronously with the generation of gravitational instabilities so that intrusions generated during these instabilities become entangled in the shear zone network.

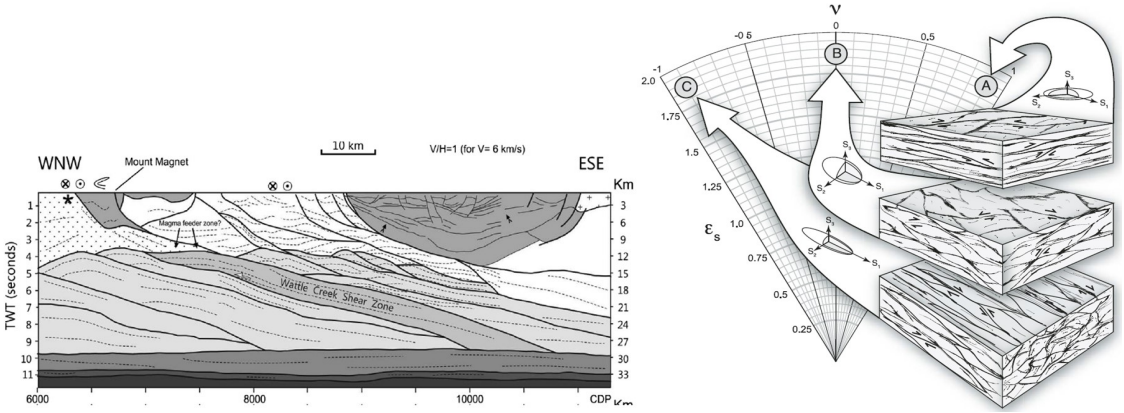

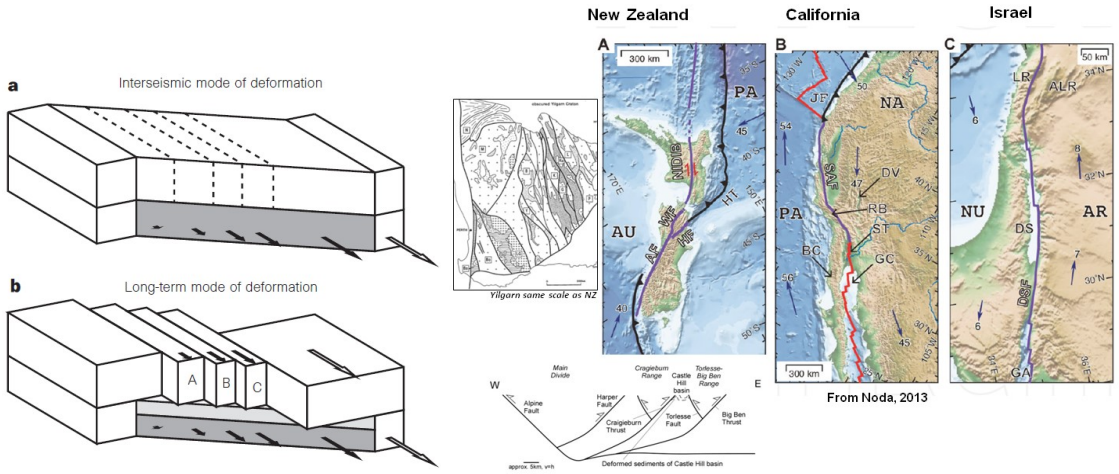

Figure 4.21. A model for tectonics in the Archean prior to plate tectonics. (a) A seismic cross section across part of the Yilgarn craton showing shear zones soling into a zone just above the Moho. (b) Basal shearing of the lithosphere produces anastomosing shear zones with horizontal modes of transport. (c) Any gradient in basal shearing produces vertical transcurrent faulting which may be listric into the Moho or the base of the lithosphere. (d) Modern versions of (c) in New Zealand, California and Palestine /Israel with the Yilgarn craton in Western Australia at the same scale.

- Any gradient in shearing velocity on the base of the lithosphere can generate more or less vertical shear zones in the lithosphere which may become listric into the sliding base of the lithosphere or into other detachments such as the Moho (Figure 4.21 c). This process is common today even in a plate tectonic environment and results in the giant transform and transcurrent faults such as the Great Alpine Fault in New Zealand, the San Andreas Fault in California and the large transcurrent fault in Palestine/Israel (Figures 4.21 d) and the Anatolian Fault in South Central Asia. We propose that the Ida Fault in the Yilgarn of Western Australia represents one of these structures. The overall result is shown as a cartoon of the Yilgarn structure in Figure 4.22.

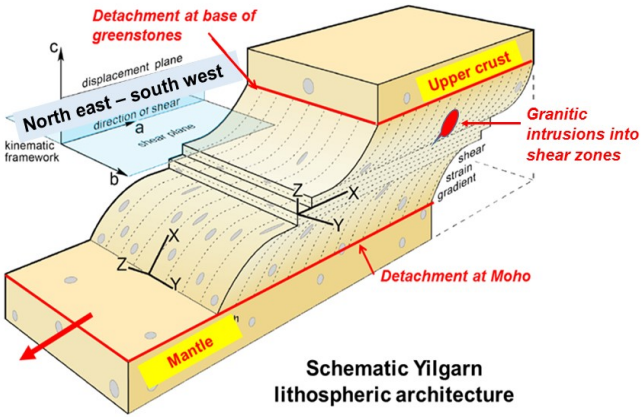

Figure 4.22. Cartoon of the lithospheric archetecture of the Yilgarn resulting from pre-plate tectonic processes.

4.7. Summary.

This chapter has been concerned with discussing the tectonic environment that is most favourable for the generation of orogenic gold deposits. We have approached this through computer simulations where deformation, fluid flow, heat transport and chemical reactions are

coupled through chemical equilibrium thermodynamics linked to physical data bases. The requirement is for large volumes of CO_2 and H_2O with associated H_2S and of course, gold in solution. Such a source is probably best found as carbonates in altered mafic rocks or as sediments. A well-established hypothesis is that such a source is to be found in crustal rocks that suffer regional metamorphism. This process sources the CO_2, H_2O, H_2S and gold from the crustal rocks in enough volume to produce high grade gold deposits but the process is slow since the volumetric flow rates of fluids are controlled by the rates at which the regional metamorphic isograds rise in the crust as a result of *conduction*. The time scale for the resulting process is likely to be measured in tens of millions of years rather than the 1 to 2 million years which seems to be an extreme upper limit for the formation of a high grade gold deposit. Also the resultant flux of fluids is dispersed and some form of accumulation and focussing of fluids is required to produce an ore body. There is also no necessary connection between such a regional metamorphic scenario and localised extensional deformation or the intrusion of alkaline igneous rocks both of which characterise deposits such as those in the Yilgarn of Western Australia.

Alternative mechanisms involve *advecting* the carbonate bearing source rocks rapidly through a temperature gradient by rapid tectonic processes. Two models appear as important. One involves the subduction of carbonate bearing rocks. Normally this is not considered to be important because the temperatures in the down-going slab are normally too low to allow decarbonation until the slab is very deep. However if rollback occurs hot mantle is rapidly brought into contact with the top of the slab resulting in simultaneous release of large volumes of CO_2 and H_2O. The process is localised both spatially and temporally with a maximum time for the event lasting about 3 million years. The event is associated with extension of the crust and the opportunity exists to produce alkaline igneous rocks arising from CO_2 induced melting.

A second related process involves rifting of a previously metasomatised lithosphere. Large volumes of CO_2 are released along the margins of the rift in an event that lasts < 5 million years. Again the process is related to extension and the opportunity exists to produce alkaline igneous rocks.

These process define clear mineral exploration concepts at the regional scale and allow some quantitative estimation of the most likely places for mineralisation relative to the timing and nature of tectonic events and the styles of structural features.

Recommended reading.

Piriz, A. R., Cela, J. J. L., and Tahir, N. A., 2009, Rayleigh-Taylor instability in elastic-plastic solids: Journal of Applied Physics, v. 105, no. 11.

Gonzalez

Gorczyk, W, and Vogt, K. 2014, Tectonics and melting in intra-continental settings: Gondwana Research. http://dx.doi.org/10.1016/j.gr.2013.09.021